RRH: INTRATEST TRACE ELEMENT GEOCHEMISTRY

LRH: HUPP AND FEHRENBACHER

INTRATEST TRACE ELEMENT VARIABILITY IN POLAR AND SUBPOLAR PLANKTIC FORAMINIFERA: INSIGHTS INTO VITAL EFFECTS, ONTOGENY, AND BIOMINERALIZATION PROCESSES

BRITTANY N. HUPP[1,2,3*] AND JENNIFER S. FEHRENBACHER[2]

[1]4400 University Dr. MS2B3, Department of Atmospheric, Oceanic and Earth Sciences, George Mason University, Fairfax, VA 22030 USA

[2]Ocean Administration Building, 101 SW 26th St. College of Earth, Ocean, and Atmospheric Sciences, Oregon State University, Corvallis, OR 97331 USA

[3]NOAA Climate and Global Change Postdoctoral Fellowship Program, CPAESS, UCAR, Boulder, CO, USA

*Corresponding Author: Brittany N. Hupp (bhupp@gmu.edu)

ABSTRACT

To use planktic foraminiferal tests as paleoproxy substrates, it is necessary to delineate environmental versus biological controls on trace element incorporation. Here we utilize laser-ablation inductively coupled plasma mass spectrometry (LA-ICP-MS) to explore interspecies, chamber-to-chamber, and intratest trace element (i.e., Mg, Na, Sr, Ba, Mn, Zn) variability in thickly-calcified specimens of the polar and subpolar planktic foraminifera *Neogloboquadrina incompta*, *N. pachyderma*, and *Turborotalita quinqueloba* collected from plankton tows in the Northern California Current. Among the study taxa, test Mg/Ca, Na/Ca, and Sr/Ca are likely dominantly controlled by depth habitat. The neogloboquadrinids record higher Ba/Ca and Mn/Ca, and also show positive covariance between these elements, possibly due to calcifying in an oxygen-depleted marine snow microhabitat. Trace elements are found to be more enriched in the lamellar calcite than the outer chamber wall dominated by gametogenic crust. The data presented herein provide insight into potential vital effects, paleoproxy considerations, ontogeny, and biomineralization processes.

INTRODUCTION

The trace element geochemistry (TE/Ca) of foraminifera varies as a function of seawater composition, the physical conditions of the water in which they are calcifying, and the biological conditions during calcification (e.g., Lea et al., 1999; Erez, 2003; Russel et al., 2004; Katz et al., 2010; Allen et al., 2016; de Nooijer et al., 2017; Evans et al., 2018). Thus, great efforts have been made to quantitatively constrain relationships between foraminiferal test TE/Ca geochemistry and the conditions of the foraminifer's living environment, as a means for paleoenvironmental reconstruction. While some foraminiferal TE/Ca paleoproxies have been rigorously studied, such as Mg/Ca as a paleotemperature proxy (Nürnberg, 1995, Nürnberg et al., 1996; Lea et al., 1999; Anand et al., 2003; Russell et al., 2004; Martínez-Botí et al., 2011; Hönisch et al., 2013; Holland et al., 2020), incorporation of other TEs into foraminiferal calcite is less well-understood and represent new pathways of needed exploration. In addition to understanding the environmental controls on TE incorporation, it is equally important to constrain how biological processes modulate TE geochemistry. Biological processes that influence test geochemistry, broadly referred to as "vital effects" (Niebler et al., 1999; de Nooijer et al., 2014; Schiebel and Hemleben, 2017), can distort primary environmental signals, thus interfering with paleoreconstructions reliant upon test geochemistry. For example, trace element geochemistry may differ from chamber-to-chamber or when examining profiles of TEs across a chamber wall (Eggins et al., 2003; Steinhardt et al., 2014, Steinhardt et al., 2015; Davis et al. 2020; Hupp and Fehrenbacher, 2023). Furthermore, ontogenetic processes, such as test thickening observed in several species of planktic foraminifera syn- and post-gametogenesis, have been shown to impart different geochemical signatures in

different portions of the test wall (see Table 1 of Hupp and Fehrenbacher, 2023 and references therein). Recognizing intratest variability is informative to identifying potential vital effects, as well as providing insight into ontogeny and biomineralization processes (Hathorne et al., 2003; Eggins et al., 2003; Davis et al., 2020). Fossilized test TE/Ca variability can be further confounded by the addition of diagenetic calcite, which varies even more from primary foraminiferal calcite compositions (e.g., Boussetta et al., 2011; Kozdon et al., 2013; Edgar et al., 2015).

Recent advances in *in situ* technologies such as laser-ablation inductively coupled plasma mass spectrometry (LA-ICP-MS) provide a unique opportunity to investigate intratest trace element variability. LA-ICP-MS analysis allows for quantifying TEs in individual foraminifera in a population of specimens (i.e., intertest variability). By analyzing micron-scale intratest variability using LA-ICP-MS, one can also identify potential vital effects and investigate other mechanisms responsible for trace element incorporation in foraminifera (Hathorne et al., 2003; Eggins et al., 2003; Sadekov et al., 2010; Davis et al., 2020). This is necessary to identify intertest and intratest TE variability that potentially confound "averaged" TE measurements used in paleoreconstructions, as is the case in more traditional, pooled, whole-test 'bulk' analytical techniques, such as solution analysis.

LA-ICP-MS is commonly used to investigate TE geochemistry in modern planktic foraminiferal species (e.g., Hathorne et al., 2009; Steinhardt et al., 2015; Davis et al., 2020), however, these investigations predominantly focus on tropical, subtropical, and transitional species. Here, we explore the intratest variability of polar and subpolar modern planktic foraminiferal species, specifically *Neogloboquadrina incompta* (Cifelli, 1961), *Neogloboquadrina pachyderma* (Ehrenberg, 1861), and *Turborotalita quinqueloba* (Natland, 1938), to bolster their usage as geochemical paleoproxy substrates. Specimens investigated in this study were collected

from plankton tow samples throughout the Northern California Current region under a wide range of environmental conditions between 2011 and 2022. All specimens were dead upon collection as identified by their thickly-crusted test walls and, in recently collected samples, the absence of remnant cytoplasm. Only encrusted specimens were examined, as the presence of crust indicates the end or near-end of an individual's life-cycle, and thus are likely more representative of fossilized specimens found on the seafloor (Bé and Lott, 1964; Bé, 1980; Caron et al., 1990; Davis et al., 2020). By characterizing the intratest variability of crusted (i.e., dead) specimens collected across a wide range of conditions in the uppermost surface ocean, we aim to provide a foundation from which future trace element studies focused on polar and subpolar planktic foraminifera collected from sediment traps and the seafloor can be compared. Furthermore, this study illustrates the wide range of approaches that can be taken to investigating foraminiferal geochemistry when using LA-ICP-MS data. This study provides insight into vital effects and trace element incorporation into the tests of polar and subpolar planktic foraminifera taxa independent of potential trace element heterogeneity associated with travel through the water column (e.g., scavenging; Davis et al., 2020) or early diagenesis upon the seafloor (e.g., Branson et al., 2015).

HYDROGRAPHIC SETTING

Study specimens were collected via surface plankton tow from offshore sites throughout the Northern California Current (NCC) region, ranging from northern California to the border between Washington (USA) and Canada (**Fig. 1**). This region of the Northeast Pacific Ocean is characterized by a relatively narrow, deep continental shelf (0 to 200 m) and a steep continental slope that transitions into deep (> 2500 m) water 25-50 km offshore. A well-developed seasonal

oxygen minimum zone (OMZ, 600-1000 m) associated with North Pacific Intermediate Water exists offshore (e.g., Paulmier and Ruiz-Pino, 2009; Pierce et al., 2012). As in many other eastern boundary ocean margins, upwelling along the margin is a highly seasonal phenomenon driven by shifts in wind strength and direction (Barth and Wheeler, 2005). During spring and summer, this region experiences strong upwelling caused by prevailing northerly winds that induce Ekman transport of deeper water from the shelf break onto the continental shelf (e.g., Kirincich et al., 2005; Perlin et al., 2005). Fall and winter display starkly different conditions, with southerly, downwelling-favorable winds, large swells, high wave energies nearshore, and the arrival of moisture-laden storms (Kniskern et al., 2011). Environmental variability due to seasonal upwelling is further overprinted by longer-term oscillations such as El-Niño Southern Oscillation and the Pacific Decadal Oscillation. Collectively, these features create a dynamic region with diverse conditions under which regional planktic foraminifera calcify (Ortiz and Mix, 1992; Taylor et al., 2018; Lane et al., 2023).

MATERIALS AND METHODS

PLANKTON TOWS AND STUDY SPECIMENS

Plankton tows were collected from several sites (**Fig. 1**) during a series of cruises conducted between 2011 and 2022. Vertical tows were conducted from 100 m depth to the surface using a 150 μm mesh net. Most tows were obtained during NOAA-led fisheries survey cruises, where samples were preserved using NaOH-buffered formalin immediately upon collection and stored in a sample archive (Feinberg and Peterson, 2003). Planktic foraminiferal tests were removed from

138 archived tows, rinsed with DI water upon removal, and stored on micropaleontological slides until
139 further cleaning was conducted in preparation for geochemical analysis. In addition to tests from
140 archived tows, additional tows were collected by the authors where tests were immediately
141 removed from tows, rinsed with DI water, and stored on micropaleontological slides, without any
142 exposure to preservative chemicals. In total, specimens examined herein originate from 39 discrete
143 tows collected across 29 different sites over a period of 11 years. Metadata for each test examined,
144 including tow location (site name, latitude, longitude) and archived (preserved in buffered
145 formalin) versus recently collected (never exposed to preservatives) status is detailed in the
146 **Supplementary Appendix 1**.

147 Specimens of *N. incompta* (N = 92)*, N. pachyderma* (N = 55), and *T. quinqueloba* (N = 42)
148 were selected for individual foraminifer geochemical analysis. All three study taxa are asymbiotic;
149 however, *T. quinqueloba* is a spinose species whereas the neogloboquadrinids are non-spinose
150 (Schiebel and Hemleben, 2017). Specimens selected for analysis were limited to heavily-calcified
151 tests (i.e., clearly apparent crusts) where it is inferred or confirmed that the specimens were dead
152 upon collection. For archive specimens, dead specimens were inferred based upon evidence of a
153 clearly apparent gametogenic crust (see fig 1. in Hupp and Fehrenbacher, 2023 for further
154 description of crusted versus uncrusted individuals). For the recently collected specimens, dead
155 specimens were heavily-calcified and lacked cytoplasm.

156

157 TEST PREPARATION AND CLEANING

158

159 Study specimens underwent an oxidative cleaning process to remove remnant organic matter
160 and detritus (Mashiotta et al., 1999) which consisted of 1) rinsing the tests with methanol, 2)

rinsing the tests with ultrapure milliQ water three times 3) submerging tests in a 1:1 solution of 30% H_2O_2 buffered with 0.1 M NaOH and placing vials containing the tests and solution in a warm (~65°C) water bath for 10 minutes, and lastly, 4) removing the H_2O_2-NaOH solution and rinsing the tests with milliQ water three times. While previous studies submerge the tests for 30 minutes, the water bath time was decreased to 10 minutes to prevent test dissolution (Bonnin et al., 2019).

LA-ICP-MS

Trace element geochemistry was determined via laser-ablation inductively coupled plasma mass spectrometry (LA-ICP-MS). Tests were analyzed with a Thermo Scientific iCAP RQ quadrupole ICP-MS coupled to an Applied Spectra RESOlution (193 nm) laser-ablation system housed in the Keck Collaboratory for Plasma Spectrometry at Oregon State University. While ten isotopes were measured during analysis, seven isotopes are examined herein: ^{24}Mg, ^{23}Na, ^{88}Sr, ^{138}Ba, ^{55}Mn, ^{66}Zn, and ^{43}Ca. Isotopes were measured using a rapid peak-hopping method where Mn, Zn, Ba were assigned dwell times of 0.05 s, Na a dwell time of 0.04 s, Sr and Mg dwell times of 0.02 s, and Ca a dwell time of 0.01 s (total sweep time: 0.29 s). Analysis spots were ablated from the outer chamber wall (the test surface) through the chamber wall. For the neogloboquadrinids, laser energy was set to 4.0 mJ attenuated by 87.5% whereas for *T. quinqueloba* the laser energy was reduced to 3.0 or 3.5 mJ, also attenuated by 87.5%. Circular spot sizes range from 24 to 50 μm and were adjusted for each specimen to maximize the ablated area. Repetition rates were adjusted between 5 and 6 Hz to optimize laser profiles. Individual laser analyses were conducted on the F0, F1, F2, F3, and F4 chambers of *T. quinqueloba* and the F0, F1, F2, and F3 chambers for *N. incompta* and *N. pachyderma*. In rare cases, due to test orientation,

184 the oldest chamber in the outer whorl (F4 and F3 for *T. quinqueloba* and the neogloboquadrinids,
185 respectively) was not accessible to be analyzed. Repeat analyses were conducted on at least one
186 chamber per specimen to assess reproducibility (**Supplemental Table 1**).

187 Three standard reference materials were measured bracketing every 10 to 12 specimens (i.e.,
188 every 50 to 72 test ablation spots across 10 to 12 continuous profiles), including the glasses NIST
189 610 and NIST 612, and the compressed-powder USGS standard MACS-3. Each standard was
190 ablated for 60 s using a repetition rate of 6 Hz on a spot size of 50 μm with a laser energy of 5 mJ
191 attenuated by 50%. All TE/Ca were calibrated using the NIST 610 and 612 glasses, aside from
192 Na/Ca which was calibrated using NIST 610 and MACS-3 due to a consistent concentration of Na
193 within NIST glass standards. Elemental calibrations of standard reference materials measured
194 throughout the analysis sessions yielded $r^2 \geq 0.99$.

195 Data was processed with the Python package *LAtools* (Branson et al., 2019) following
196 established data reduction protocols (Longerich et al., 1996). Data reduction involves despiking
197 and signal smoothing to remove outliers in the laser spectra, evaluation and correction for any drift
198 observed in the standard measurements throughout the analysis session, and removal of average
199 background counts from each data point. Data output from this process produces individual
200 specimen files, where each spot measurement composes a distinct section of the full spectrum, as
201 well as mean TE/Ca for each spot analysis, normalized to known TE/Ca concentrations of the
202 standards (**Supplemental Fig. 1**; Jochum et al., 2011). Whole-test averages and individual
203 chamber averages of all TEs for each specimen are reported in **Supplemental Appendix 2**. For
204 chambers where multiple measurements were taken, the replicate measurements were averaged to
205 produce the chamber values reported in **Supplemental Appendix 2**.
206

RESULTS

INTERSPECIES WHOLE TEST AVERAGE TE/CA VARIABILITY

The range of whole-test average TE/Ca compositions for the study specimens provides context for further investigation of the intratest geochemistry in these species (**Fig. 2, Table 1**). Whole-test averages were determined by taking the mean of the average chamber measurements from each chamber in the outer whorl (**Fig. 2A**). Note that where multiple measurements were taken within a single chamber, those measurements were averaged to determine a chamber mean value before being used to calculate the whole-test average. It is recognized that the whole-test average as described here is technically an interpolated average, as we are calculating the mean of several discrete measurements taken from chambers in the outer whorl as opposed to dissolving and analyzing the entire test, as done in solution analyses. However, comparing the "whole test" value as measured by solution-based ICP-MS and interpolated by laser-based ICP-MS result in negligible differences (Fehrenbacher et al., 2020). We also recognize that while much of the interspecies variability is directly tied to environmental variability during specimen collection/period of calcification, the whole test TE/Ca geochemistry provides context for the subsequent discussion of intratest TE/Ca variability. Furthermore, examination of whole-test TE/Ca distributions provides insight into elements that are potentially modulated by environmental conditions. For example, TEs that do not vary significantly may suggest that these TEs are not strongly impacted by calcification conditions (e.g., Ba/Ca in *T. quinqueloba*; **Fig. 2E**).

Here we describe the whole-test average distributions by examining the distribution mean (**Table 1**) as well as the distribution range, as defined by the maximum whisker value minus the

minimum whisker value of the boxplots shown in **Figure 2**. *Neogloboquadrina incompta* generally records the lowest average Mg/Ca, Na/Ca, and Sr/Ca, followed by *N. pachyderma*, and *T. quinqueloba* (**Fig. 2B-D**). The range of the distributions is fairly consistent between all taxa for Mg/Ca (~3 mmol/mol) and Sr/Ca (~0.25 mmol/mol), but the Na/Ca range increases from: ~6 mmol/mol in *N. incompta;* to 13 mmol/mol in *N. pachyderma;* and to 22 mmol/mol in *T. quinqueloba*, respectively. Interspecies TE/Ca differences are more irregular when comparing Ba, Mn, and Zn (**Fig. 2E-G**). While all taxa exhibit similar Ba/Ca minima, *N. incompta* exhibits the largest range of Ba/Ca values (41 µmol/mol), followed by *N. pachyderma* (16 µmol/mol), and lastly with the smallest range, *T. quinqueloba* (5 µmol/mol) (**Fig. 2E**). *Neogloboquadrina incompta* also exhibits a larger range of Mn/Ca values (25 µmol/mol) compared to *N. pachyderma* (7 µmol/mol) and *T. quinqueloba* (11 µmol/mol) (**Fig. 2F**). The inner quartile ranges are comparable among all three taxa for Zn/Ca, but the full range of whole test values is largest in *N. pachyderma* (977 µmol/mol), followed by *T. quinqueloba* (728 µmol/mol), and lastly, *N. incompta* (586 µmol/mol). *Neogloboquadrina pachyderma* also records higher Zn/Ca values on average than *T. quinqueloba* and *N. incompta* (**Fig. 2G**).

CHAMBER-TO-CHAMBER TE/CA VARIABILITY

To explore how TE/Ca may change through ontogeny, chamber-to-chamber TE/Ca averages are compared to one another by mean centering the TE/Ca data (i.e., whole test average TE/Ca is subtracted from each chamber average; **Fig. 3A**). By normalizing each chamber average by the test average, the range of chamber-to-chamber variability can be examined while

252 removing variability that could be more directly attributed to calcification under different
253 environmental conditions.

254 For all three taxa, the Mg/Ca composition decreases in each successively-added chamber
255 in the outer whorl, with the youngest chamber (F0) exhibiting the lowest values found in the outer
256 whorl (**Fig. 3B, E, H**). The F4 chamber of *T. quinqueloba* does not seem to follow the intratest
257 pattern (**Fig. 3H**), however this could be an artifact, as not all F4 chambers could be analyzed in
258 this taxon. Ratios of Na/Ca and Sr/Ca show minimal chamber-to-chamber variability in *N.*
259 *pachyderma* (**Fig. 3F, G**) and *T. quinqueloba* (**Fig. 3I, J**). However, in *N. incompta*, the F0
260 chamber records consistently higher Na/Ca than all other chambers in the outer whorl (**Fig. 3C**).
261 A consistent increase in Sr/Ca is observed with each successively younger chamber in the outer
262 whorl of *N. incompta* (**Fig. 3D**). The ratio of Ba/Ca differs little between chambers in *N. incompta*
263 (**Fig. 4A**), however the older chambers (i.e., F2, F3) tend to record slightly higher Ba/Ca values
264 than the ultimate and penultimate chambers of *N. pachyderma* and *T. quinqueloba* (**Fig. 4D, G**).
265 A similar pattern of decreasing TE/Ca content in each sequentially-added chamber is observed
266 with Mn/Ca in *N. pachyderma* (**Fig. 4E**) and *T. quinqueloba* (**Fig. 4H**), whereas *N. incompta* shows
267 only a relative Mn/Ca depletion in the F0 chamber (**Fig. 4B**). The neogloboquadrinids exhibit an
268 opposite pattern with Zn/Ca where Zn incorporation increases with each progressively added
269 chamber (**Fig. 4C, F**). Conversely, *T. quinqueloba* shows a progressive decrease in Zn
270 incorporation with each progressively-added chamber, aside from the ultimate F0 chamber (**Fig.**
271 **4I**).

272

273 INTRATEST TE/CA VARIABILITY

274

In addition to characterizing the chamber-to-chamber variability, the range of values measured from individual chambers within a single test is also explored (**Fig. 5**). The intratest range is calculated by subtracting the lowest chamber average value of those measured in the outer whorl from the highest chamber average value of outer whorl chambers in a single specimen (e.g., **Fig. 5A**). Here, the medians of the boxplot distributions (**Fig. 5**) will be discussed, as some TE/Ca exhibit several outliers influencing the distribution mean. The median intratest range of Mg/Ca values ~0.8 mmol/mol in the neogloboquadrinids, however the distribution of ranges exhibits a greater spread for *N. pachyderma* than for *N. incompta* (**Fig. 5B**). *Turborotalita quinqueloba* exhibits a median intratest Mg/Ca range of ~1.6 mmol/mol. The median of the intratest Na/Ca range increases from 2.0 mmol/mol in *N. incompta* to 3.4 mmol/mol in *N. pachyderma* to 8.8 mmol/mol in *T. quinqueloba*, and the distribution spread of intratest ranges increase in the same taxa order (**Fig. 5C**). Distributions of intratest Sr/Ca ranges are very similar among the three study taxa, with a median intratest range of ~0.1 mmol/mol (**Fig. 5D**). Intratest Ba/Ca ranges show an opposite pattern among taxa as observed in Na/Ca (**Fig. 5E**). The median of intratest Ba/Ca ratios was found to be 6.4 µmol/mol in *N. incompta*, 4.7 µmol/mol in *N. pachyderma*, and 2.4 µmol/mol in *T. quinqueloba*. The boxplot distribution of intratest Ba/Ca ranges shows the highest maximum value in *N. incompta* (36.6 µmol/mol), followed by *N. pachyderma* (18.1 µmol/mol), and lastly, *T. quinqueloba* (9.9 µmol/mol). For Mn/Ca, *T. quinqueloba* shows the highest median internal variability (6.6 µmol/mol), followed by *N. incompta* (6.3 µmol/mol), and *N. pachyderma* (3.0 µmol/mol), however, the distribution of Mn/Ca intratest ranges recorded by *N. incompta* shows the greatest spread (**Fig. 5F**). Conversely, the highest median range of intratest Zn/Ca is recorded by *N. pachyderma* (357 µmol/mol), followed by *T. quinqueloba* (194 µmol/mol), and *N. incompta*

297 (111 μmol/mol), with *N. pachyderma* exhibiting the greatest variability of intratest ranges (**Fig.**
298 **5G**).

299 Intratest TE/Ca variability, characterized by the intratest range and standard deviation of
300 average chamber measurements in the outer whorl, can be compared to the whole-test TE/Ca value
301 of an individual specimen to determine if intratest variability fluctuates consistently with
302 increasing or decreasing TE/Ca content (**Table 2**). Intratest Mg/Ca variability shows a strong
303 (range $r^2 = 0.67$, and standard deviation or "SD" $r^2 = 0.68$) and moderately strong (range and SD
304 $r^2 = 0.58$) positive relationship with whole-test Mg/Ca values in *N. incompta* and *N. pachyderma*,
305 respectively. No correlation is found between intratest Mg/Ca variability and the whole-test
306 average value in *T. quinqueloba*. *Neogloboquadrina incompta* exhibits a moderate positive
307 correlation (range $r^2 = 0.53$, SD $r^2 = 0.54$) between intratest Na/Ca variability and the whole-test
308 value, whereas *N. pachyderma* (range and SD $r^2 = 0.36$) and *T. quinqueloba* (range $r^2 = 0.32$, SD
309 $r^2 = 0.33$) exhibit only weak positive correlations. No relationship is found between Sr/Ca intratest
310 variability and the whole-test Sr/Ca value in any of the three study taxa. Whole-test Ba/Ca shows
311 a very strong positive correlation with intratest variability in *N. pachyderma* (range $r^2 = 0.98$, SD
312 $r^2 = 0.99$), and a strong positive relationship in *N. incompta* (range and SD $r^2 = 0.64$) and *T.*
313 *quinqueloba* (range $r^2 = 0.75$, SD $r^2 = 0.76$). A strong positive relationship is found in *N. incompta*
314 (range $r^2 = 0.70$, SD $r^2 = 0.72$) and *T. quinqueloba* (range $r^2 = 0.77$, SD $r^2 = 0.78$) when comparing
315 intratest Mn/Ca variability to whole-test values, and a moderate to weak positive correlation is
316 found in *N. pachyderma* (range $r^2 = 0.41$, SD $r^2 = 0.39$). Moderate positive correlations are also
317 found between intratest Zn/Ca variability and whole-test values in *T. quinqueloba* (range $r^2 = 0.62$,
318 SD $r^2 = 0.61$) and *N. pachyderma* (range $r^2 = 0.51$, SD $r^2 = 0.49$), with a weak correlation observed
319 in *N. incompta* (range $r^2 = 0.37$, SD $r^2 = 0.38$).

INTRACHAMBER TE/CA VARIABILITY

Laser ablation was conducted from the outside of the test through to the inner chamber wall allowing for individual depth profiles to be used to assess how the geochemistry of the test changes through the test wall (e.g., **Fig. 6**). All specimens examined for this study were chosen because they appeared to be thickly calcified, and all three species are known to exhibit a gametogenic crust (Schiebel and Hemleben, 2017; Pearson and Kucera, 2018). The inner versus outer calcite TE/Ca data are compared to evaluate if trace elements vary between the inner chamber wall and outer gametogenic crust (**Figs. 6, 7**). For simplicity, we assume the first half of a given depth profile (the outer calcite) is dominantly composed of crust calcite; the second half of the same depth profile, represents dominantly the inner chamber calcite or "lamellar" calcite (cf., Hupp and Fehrenbacher, 2023; **Fig. 6B**). If there is little to no difference in the average of these two values (e.g., data points sit upon a 1:1 line, **Figs. 6C, 7**), we assume that TEs do not vary greatly between the outer crust and the inner chamber wall. Conversely, if a chamber exhibits higher TEs in the crust or inner chamber wall, data points will either plot above or below the line of equality, respectively. While there is some variability in the amount of gametogenic calcite precipitated at the end of ontogeny, the 50% rule is an appropriate approximation (Bé, 1980; Ariwaka, 1983; Mulitza et al., 1997; Bauch et al., 2002; Simstich et al. 2003; Bolton and Marr, 2013; Hupp and Fehrenbacher, 2023). Definitively quantifying the amount of early ontogenetic versus gametogenic crust calcite in our study populations (N = 189) would require laborious analyses (e.g., thin sectioning specimens for EMPA and SEM imaging) which is outside of the scope of this study.

For all trace elements, aside from Ba, all three taxa show greater enrichment in TEs in the inner 50% of the spectrum (i.e., the lamellar calcite) compared to the outer 50% of the same spectrum (i.e., the outer crust; **Fig. 7**). Deviation from the line of equality is greatest in Mg/Ca, Na/Ca, and Sr/Ca, whereas the inner chamber wall shows only minor enrichments in Mn/Ca and Zn/Ca compared to the crust, aside from large deviations observed in the Zn/Ca of *T. quinqueloba* (**Fig. 7R**). Ratios of Ba/Ca are also heavily enriched (in some cases by >200%) in the inner chamber walls of the neogloboquadrinids, yet *T. quinqueloba* shows a minor enrichment of Ba in the crust relative to the lamellar calcite of the inner test wall due to a few high-Ba specimens (**Fig. 7P**).

PATTERNS IN TE/CA COVARIANCE

As potential controls on TE incorporation are considered, it is helpful to evaluate patterns in TE covariance. **Figure 8A-C** shows covariance matrices for the whole-test TE/Ca values of our study specimens, separated by taxon. This results section will focus upon discussing moderate and strong relationships, as several elements covary at $r^2 < 0.40$. For *N. incompta*, Mg/Ca moderately positively covaries with Na/Ca ($r^2 = 0.47$) and Sr/Ca ($r^2 = 0.45$) on the whole-test average scale (**Fig. 8A**). Moderate positive relationships are also found between Ba/Ca and Mn/Ca ($r^2 = 0.52$) as well as Ba/Ca and Zn/Ca ($r^2 = 0.43$). For *N. pachyderma*, a strong positive relationship is observed between Na/Ca and Sr/Ca ($r^2 = 0.64$) (**Fig. 8B**). Ratios of Na/Ca also moderately positively covary with Mg/Ca ($r^2 = 0.50$), Ba/Ca ($r^2 = 0.57$), and Mn/Ca ($r^2 = 0.47$). Moderate positive covariations are found between Mg/Ca and Sr/Ca ($r^2 = 0.45$), Mg/Ca and Ba/Ca ($r^2 = 0.47$), Ba/Ca and Mn/Ca ($r^2 = 0.48$), and Mn/Ca and Zn/Ca ($r^2 = 0.40$) in this taxon. *Turborotalita quinqueloba* exhibits the least number of correlations between trace elements, with Mg/Ca and Na/Ca exhibiting a moderate

365 positive correlation ($r^2 = 0.49$), and Sr/Ca and Ba/Ca exhibiting a strong negative correlation ($r^2 =$
366 -0.80) (**Fig. 8C**).

367 In addition to investigating covariance in TEs on the whole-test scale, the TE covariation in
368 individual chambers is also explored (**Fig. 8D-F**). At first glance, there are many more significant
369 (p-value ≤ 0.05) relationships at the chamber level. For example, some level of significant positive
370 covariance is found among all elements studied in the neogloboquadrinids (**Fig. 8D, E**). Of note,
371 *N. incompta* exhibits moderate positive covariance between Mg/Ca, Na/Ca, Sr/Ca, and Ba/Ca with
372 r^2 ranging from 0.50 and 0.66 for each of the combinations of TE comparisons (**Fig. 8D**). Moderate
373 positive relationships also exist between Mn/Ca and Na/Ca ($r^2 = 0.42$), as well as Mn/Ca and Ba/Ca
374 ($r^2 = 0.43$). *Neogloboquadrina pachyderma* also shows moderate positive correlations between
375 Mg/Ca, Na/Ca, and Sr/Ca ($0.44 \leq r^2 \leq 0.51$; **Fig. 8E**). However, the strongest positive relationships
376 in this taxon are found between Ba and Mn ($r^2 = 0.73$) and Mn and Zn ($r^2 = 0.71$), with Ba and Zn
377 exhibiting a moderate positive relationship ($r^2 = 0.47$). Comparisons of chamber TEs for *T.*
378 *quinqueloba* result in more significant covariations than found on the whole-test scale, the
379 strongest being between Mg and Na ($r^2 = 0.57$) and Na and Ba ($r^2 = 0.52$; **Fig. 8F**).
380
381 # DISCUSSION
382
383 ## WHOLE TEST TE/CA GEOCHEMISTRY OF POLAR AND SUBPOLAR PLANKTIC FORAMINIFERA
384
385 Interesting differences in whole-test trace element geochemistry are identified among the
386 three study species (**Fig. 2, Table 1**). For example, the whole-test Mg/Ca, Na/Ca, and Sr/Ca
387 systematically increase when comparing *N. incompta* to *N. pachyderma* to *T. quinqueloba*,

388 respectively (**Fig. 2**). These interspecies differences are likely reflective of differences in living
389 depth habitat in the study region where *N. incompta* prefers the deepest depth habitat of the three
390 study taxa, and *T. quinqueloba* prefers the shallowest. Magnesium is known to be incorporated at
391 greater concentrations into the foraminiferal crystal lattice when the test is grown under higher
392 temperatures (Nürnberg et al., 1996; Lea et al., 1999; Anand et al., 2003; Russell et al., 2004;
393 Martínez-Botí et al., 2011; Hönisch et al., 2013; Holland et al., 2020). The highest whole test
394 Mg/Ca values are found in *T. quinqueloba*, suggesting that they live closest to the relatively
395 warmer sea surface, and the lowest Mg/Ca values are found in *N. incompta,* suggesting that they
396 prefer a deeper, cooler depth habitat (**Fig. 2B**). If we are to assume that the Mg/Ca composition of
397 the three study taxa represents their preferred depth habitat, then this general pattern in relative
398 depth habitat among the three study taxa are consistent with those observed in much of the Nordic
399 Seas (Simstich et al., 2003), but differ from those characterized for the subtropical eastern North
400 Atlantic (Rebotim et al., 2017).

401 Foraminiferal Na/Ca has been identified as a potential paleosalinity proxy, where test
402 Na/Ca compositions positively covary with salinity (Wit et al., 2013; Mezger et al., 2016; Bertlich
403 et al., 2018; Bertlich et al., 2021; Watkins et al., 2021) or as a proxy for the major ion chemistry
404 of seawater on long timescales (Zhou et al., 2021; Gray et al., 2023). Among the data presented
405 herein, there is a systematic increase in Na/Ca where not only the whole-test value but also the
406 range of whole test Na/Ca values progressively increase from *N. incompta* to *N. pachyderma* to *T.*
407 *quinqueloba* (**Fig. 2C**). This observation contradicts the current understanding of foraminiferal
408 Na/Ca and salinity. In the Northern California Current region, salinity is found to generally
409 increase with depth (Ortiz et al., 1996; Lane et al., 2023) suggesting that one should expect to find
410 a decrease in Na/Ca values when comparing *N. incompta* to *N. pachyderma* to *T. quinqueloba*,

411 respectively. However, existing studies on the Na/Ca composition of several planktic foraminiferal
412 taxa have found distinct differences in species-specific Na/Ca-salinity calibrations (e.g., see figure
413 7 in Bertlich et al., 2021). For example, tropical species *Trilobatus sacculifer* incorporates Na at
414 lower rates than polar taxon *N. pachyderma* (Allen et al., 2016; Bertlich et al., 2018; Mezger et al.,
415 2018; Bertlich et al., 2021). Deviation from predicted interspecies differences in Na/Ca
416 composition with inferred depth habitat is most likely due to interspecies differences in Na
417 partitioning. Despite the three study species not following the predicted pattern of decreased Na/Ca
418 content with shallower depth habitats, *T. quinqueloba* does exhibit the largest range of Na/Ca
419 values, supporting the interpretation of a shallower depth habitat where salinity conditions can be
420 highly variable. All three taxa show moderate positive relationships between Mg and Na in the
421 whole-test and individual chamber scale, providing support for the interpretation of temperature
422 and salinity changes with depth habitat being the dominant controls on the modulation of these
423 elements, or, more generally, that Mg and Na incorporation mechanisms are potentially linked
424 (**Fig. 8**).

425 Measurements of Sr/Ca show the same systematic increase in whole test values among the
426 three taxa, in which the lowest values are found in *N. incompta* and the highest values are found
427 in *T. quinqueloba* (**Fig. 2D**). Distributions of whole-test values of Sr/Ca appear to have an abrupt
428 upper limit and a skewed distribution toward lower Sr/Ca values. This distribution architecture is
429 likely reflective of maximum Sr content in the uppermost surface ocean with greater variability of
430 Sr/Ca values found below the surface maximum. Recent compilations of Sr/Ca ratios in seawater
431 have found that Sr/Ca decreases with depth in the Pacific surface ocean (Lebrato et al., 2020),
432 although at much higher values than found in foraminiferal calcite (Allen et al., 2016), supporting
433 the linkage between depth habitat and foraminiferal Sr/Ca in the study taxa.

Barium and manganese incorporation may be reflective of habitat, more specifically potential growth in deeper, oxygen-poor waters or the influence of calcification in microhabitats during periods of higher productivity (Fritz-Endres et al., 2022). Non-spinose taxa have been found living and calcifying in marine snow particles, a habitat favorable for the incorporation of Ba and Mn (Fehrenbacher et al., 2018; Greco et al., 2019; Fritz-Endres et al., 2022; Richey et al., 2022). It is also noteworthy that upon picking and removing tests for this study, it was not uncommon to find neogloboquadrinid specimens embedded in marine snow. Barite forms within marine snow particles suggesting that the Ba in solution within particulate organic matter is highly elevated compared to ambient seawater (Dymond and Collier, 1996; Griffith and Paytan, 2012; Martinez-Ruiz et al., 2019; Carter et al., 2020; Martinez-Ruiz et al., 2020). During periods of high export productivity, more tests of non-spinose taxa can be found living in the abundant marine snow, leading to increased barium incorporation into the calcite crystal lattice (Fritz-Endres et al., 2022). Marine snow also acts as an oxygen-depleted microhabitat (Alldredge and Cohen, 1987), where redox-sensitive elements such as Mn could be more readily incorporated into the foraminiferal crystal lattice. However, Mn/Ca composition of some species may also be controlled by upwelling intensity (Davis et al., 2020). The Northern California Current is known for its exceptional seasonal fluctuations in upwelling intensity, in which the upwelling of nutrient-rich deep waters often lead to increased productivity in the surface ocean. Periods of higher productivity associated with upwelling or other factors are also associated with expanded oxygen minimum zones, thus potentially creating oxygen-depleted habitats on both the micro- (i.e., marine snow) and macro-scales. While the exact control on Ba and Mn incorporation in these planktic foraminiferal taxa is not well-constrained, there appears to be a similar control on the whole-test Ba/Ca and Mn/Ca of the neogloboquadrinids that helps to explain the covariation of whole-test Ba/Ca and Mn/Ca (*N.*

457 *incompta* $r^2 = 0.52$; *N. pachyderma* $r^2 = 0.48$; **Fig. 8A, B**). This positive relationship between Ba
458 and Mn is either similar (i.e., *N. incompta*, $r^2 = 0.43$; **Fig. 8D**) or stronger (i.e., *N. pachyderma*, $r^2 =$
459 0.73; **Fig. 8E**) when examining TE covariance within individual chambers. Ba/Ca and Mn/Ca are
460 not correlated on either the whole test or individual-chamber scale for *T. quinqueloba* (**Fig. 8C,**
461 **F**). Whole-test Mn/Ca ratios of *T. quinqueloba* are in a similar range to the neogloboquadrinids,
462 but the Ba/Ca ratios are considerably lower (**Fig. 2**). However, the Ba/Ca ratios recorded by *T.*
463 *quinqueloba* are elevated compared to most other spinose taxa (cf. Hönisch et al., 2011). As a
464 spinose foraminifera, *T. quinqueloba* is unlikely to live in a marine snow microhabitat, however
465 the elevated Ba/Ca and Mn/Ca ratios of this species may also be influenced by upwelling (Davis
466 et al., 2020).

467 Zinc incorporation has been found to be potentially reflective of productivity, oxygen
468 concentration, and/or carbonate ion concentration in benthic foraminifera (Marchitto et al., 2000;
469 Bryan and Marchitto, 2011; van Dijk et al., 2017), but is relatively understudied in planktic
470 foraminifera (Marr et al., 2013; Davis et al., 2023; Hupp and Fehrenbacher, 2023) and thus
471 incorporation mechanisms are poorly understood. Interspecies comparison of whole-test Zn/Ca
472 values in this study furthers this conundrum, as whole-test Zn/Ca does not appear to follow any
473 interspecies patterns similar to those described above for the other trace elements. However,
474 *Neogloboquadrina pachyderma* exhibits distinctly higher Zn/Ca values than the two other study
475 taxa and comparisons of average TEs in individual chambers yields a strong positive covariance
476 between Mn/Ca and Zn/Ca incorporation ($r^2 = 0.71$; **Fig. 8E**). Zinc is also a redox-sensitive
477 element that can become soluble under low oxygen conditions during microbial sulfate reduction,
478 and thus could also be reflective of calcification in a marine snow microhabitat (Davis et al., 2023).
479 Interestingly, we do not find a similar strength of relationship in our *N. incompta* population (**Fig.**

480 **8**). It is possible that *N. pachyderma* has a greater tolerance for calcifying under low-oxygen
481 conditions in which more time spent in such an environment could allow for growth under different
482 stages of the redox ladder. Dissolved manganese can be produced in hypoxic environments under
483 manganese reduction, whereas anoxic conditions are needed for sulfate reduction to occur in which
484 dissolved zinc could become available for incorporation in the calcite crystal lattice.

485 Interspecies differences in trace element incorporation provide useful insight into the
486 general ecology of the study taxa in this region. Although *N. incompta* and *N. pachyderma* are of
487 the same genus, differences in preferred depth habitat and potentially differences in marine
488 microhabitat growth regimes create distinct geochemical signatures among these two species.
489 *Turborotalita quinqueloba* also has a clearly different geochemistry than the neogloboquadrinids.
490 All three study taxa are asymbiotic; however, *T. quinqueloba* is a spinose species, whereas the
491 neogloboquadrinids are non-spinose. Despite lacking algal photosymbionts, *T. quinqueloba*
492 appears to have a shallower depth habitat (inferred from Mg/Ca ratios) compared to *N. incompta*
493 or *N. pachyderma* (Simstich et al., 2003). *Turborotalita quinqueloba* also exhibits very low Ba/Ca
494 whole test ratios (**Fig. 2**) and lacks significant relationships between Ba, Mn, and Zn (**Fig. 8**),
495 suggesting that even though it shares the asymbiotic ecology of the neogloboquadrinids, its TE/Ca
496 incorporation mechanisms may be more similar to symbiont-bearing spinose species.

497

498 ONTOGENETIC TRENDS IN TRACE ELEMENT INCORPORATION

499

500 Investigation of intratest variability can provide insight into ontogeny. For example,
501 chamber-to-chamber variability may be reflective of changing depth habitat or oceanographic
502 conditions during an individual's life cycle. While some chamber-to-chamber TE comparisons

show little to no difference between adjacent chambers, other chamber comparisons yield interesting results (**Fig. 3, 4, Table 3**). Here, chamber-to-chamber trends demonstrate that Mg content progressively decreases in sequentially younger chambers in all three study taxa (**Fig. 3B, E, H**). A similar chamber-to-chamber trend has been observed in *N. dutertrei* (Steinhardt et al., 2014; Fehrenbacher et al., 2018), but has not been previously recorded in other studies of *N. incompta* (Bolton, 2011; Davis et al., 2017) or *N. pachyderma* (Davis et al., 2017; Hupp and Fehrenbacher, 2023). Decreasing Mg could be reflective of an increasing depth of living habitat over the course of an individual's life (e.g., Meilland et al., 2021).

An enrichment in Na in the F0 chamber of *N. incompta* is evident (**Fig. 3C**). Recent studies have shown that addition of a gametogenic crust at the end of a planktic foraminifers' life can lead to an overall lower concentration in the whole-test trace element geochemistry (Eggins et al., 2003; Sadekov et al., 2005; Bolton and Marr, 2013; Davis et al., 2017; Hupp and Fehrenbacher, 2023). Examination of intrachamber TE composition supports this observation, where the inner lamellar calcite records higher TEs than the outer crust calcite (**Fig. 7**). The gametogenic crust tends to be relatively thin in the F0 chamber compared to other chambers in the outer whorl. Therefore, the Na geochemistry of the F0 chamber of crusted specimens can seem to be relatively enriched. Similar observations have been made for Na and Sr in populations of *N. pachyderma* collected from plankton tows in the Northern California Current (Hupp and Fehrenbacher, 2023).

Chamber-to-chamber trends in Sr/Ca vary markedly between species, with *N. incompta* exhibiting a decreasing trend with each additional chamber, *N. pachyderma* exhibiting an increasing trend, and *T. quinqueloba* showing no systematic trend (**Fig. 3, Table 3**), furthering the conundrum of what environmental parameter controls Sr incorporation (Lea et al., 1999; Martin et al., 1999; Stoll et al., 1999; Billups et al., 2004; Allen et al., 2016). Compilations of systematic

changes in Sr among adjacent chambers have revealed a wide range of intratest patterns (see Table 1 in Davis et al., 2020). Since the study of Davis et al. (2020), Hupp and Fehrenbacher (2023) found little change in chamber-to-chamber Sr/Ca variability in a population of crusted *N. pachyderma*, aside from an enrichment in Sr in the F0 chamber. Conversely, prior study of the non-spinose taxa *Globorotaloides hexagonus*, known to inhabit oxygen minimum zones, has shown a distinct increase in Sr incorporation with the addition of each new chamber (Davis et al., 2023). Ratios of Sr/Ca have been shown to increase with increased temperature, salinity, and carbonate ion concentration in spinose tropical to subtropical species (Allen et al., 2016). However, systematic chamber-to-chamber fluctuations in Sr/Ca could directly mimic changes in water Sr/Ca, reflective of dynamic changes in depth habitat through ontogeny.

Chamber Ba/Ca and Mn/Ca comparisons in *N. pachyderma* and *T. quinqueloba* show distinct decreasing trends in TE incorporation with ontogeny, whereas *N. incompta* exhibits relatively consistent Ba and Mn composition among chambers in the final whorl (**Fig. 4**). Differences in Ba and Mn content among chambers in *N. pachyderma* may reflect movement into and out of a marine snow calcifying environment during the ontogeny of an individual, in which chambers recording higher Ba/Ca and Mn/Ca values signal calcification in a marine snow microenvironment, where conditions are conducive for elevated TEs (Alldredge and Cohen, 1987; Fritz-Endres et al., 2022; Richey et al., 2022); however, this explanation would not extend to explain similar trends found in *T. quinqueloba*. While we do not find any chamber-to-chamber gradient in the Ba/Ca and Mn/Ca composition of *N. incompta*, the larger range of Ba and Mn whole-test values suggests that they too prefer a marine snow microhabitat. However, the lack of chamber variability may imply that individuals either spend nearly all of their adult life calcifying in marine snow when it is present or all of their life outside of marine snow.

549 Interspecies differences in Zn/Ca chamber-to-chamber trends inspire more questions;
550 Zn/Ca shows a clear increasing trend in progressively younger chambers of the
551 neogloboquadrinids, but exhibits a decreasing trend, aside from the F0 chamber, in *T. quinqueloba*.
552 These chamber-to-chamber observations could reflect changes in the carbonate ion concentration
553 of the calcifying microhabitat (Marchitto et al., 2000; van Dijk et al., 2017), with potential
554 differences between spinose and non-spinose taxa. However, the mechanism for producing such
555 differences in $[CO_3^{2-}]$ among spinose and non-spinose taxa is unclear, particularly because all taxa
556 examined in this study are asymbiotic and thus changing pH conditions in the local
557 microenvironment due to the photosynthesis of algal symbionts is not an explanation. Ratios of
558 Zn/Ca have been suggested to be sensitive to oxygen concentrations (Davis et al., 2023), whereby
559 incorporation of redox -sensitive Zn would increase when calcifying under low-oxygen conditions.
560 This relationship has been observed in *Globorotaloides hexagonus*, a species commonly found in
561 living in oxygen minimum zones (Davis et al., 2023). However, oxygen conditions are unlikely to
562 change *systematically* throughout the ontogeny, and thus is unlikely to be the cause of chamber-
563 to-chamber Zn variability in our study taxa. Zinc incorporation into planktic foraminiferal tests
564 continues to be an enigma.

565 While the causes of ontogenetic trends in TE incorporation are difficult to constrain, it is
566 interesting to consider the interspecies differences in such trends (**Table 3**). For example, one
567 would expect to potentially find similarities in ontogenetic TE incorporation among taxa of the
568 same genus, same spinose versus non-spinose affinity, or same symbiotic versus asymbiotic status.
569 However, we find little consistencies or natural groupings in chamber-to-chamber TE
570 incorporation among our study taxa aside from a consistent decrease in Mg incorporation through

ontogeny in all study taxa and similarities in systematic Zn incorporation among the neogloboquadrinids.

The range of intratest chamber measurements (e.g., **Fig. 5A**) can be used to identify more sporadic changes in environmental conditions throughout an individual's lifetime. For example, the intratest Ba/Ca range is highest in the neogloboquadrinids (**Fig. 5D**), where the intensity of export production may change during an individual's life or they may choose to only live a portion of their life calcifying in a marine snow microenvironment. Generally speaking, our data show that greater intratest Mg/Ca and Na/Ca variability is likely reflective of existence in a shallower depth habitat where temperature and salinity feature stronger fluctuations during a foraminifers' lifetime. This expected relationship tied to depth habitat is well-supported by the moderate positive correlations ($0.47 \leq r^2 \leq 0.53$) found between whole-test and individual chamber Mg/Ca and Na/Ca in our study taxa (**Fig. 8**). However, while *T. quinqueloba* records overall higher whole-test Sr/Ca values than the other two study taxa, we find that their intratest ranges are comparable to the neogloboquadrinids likely due to 1) the environmental condition(s) that regulate Sr incorporation not changing much in their depth habitat over the short timescale of an individual foraminifers lifetime or 2) a general insensitivity to changing Sr incorporation. Greater intratest Ba/Ca and Mn/Ca in the neogloboquadrinids and, in the case of *N. pachyderma*, Zn/Ca variability is reflective of ontogeny lived in a deeper depth habitat, likely intersecting with the oxygen minimum zone, where fluctuations in export production and oxygen saturation modulate trace element incorporation into the foraminiferal crystal lattice over an individual's lifetime. Further characterization of the preferred depth habitat of these taxa in the Northern California Current will strengthen our understanding of these geochemical-environmental relationships.

In addition to examining chamber-to-chamber variability to delineate ontogenetic controls on trace element incorporation, we can investigate how trace elements vary with depth through the chamber wall. Previous studies have investigated either a few individuals or a single population of tests to examine how test trace element geochemistry may change with the addition of gametogenic crust (e.g., Table 1 in Hupp and Fehrenbacher, 2023). However, the dataset presented herein allows for investigation into the potential for consistent patterns in the trace element differences between the gametogenic crust and early ontogenetic calcite in individuals grown under a wide range of environmental conditions. Here we find that for all three study taxa and nearly all trace elements examined herein, the inner chamber wall (i.e., dominantly lamellar calcite) has consistently higher trace element compositions than the outer chamber wall, dominated by the gametogenic crust (**Fig. 7**). This observation indicates that the biomineralization pathway for precipitating the crust post- or syn-reproduction differs from the "normal" biomineralization mechanism used for growing a test throughout the vast majority of a foraminifers life. While the gametogenic crusting process has been found to occur quickly (on the scale of hours to days; Bé, 1980), it is possible that rapid calcification rates could be linked to lower TE incorporation. However, studies of symbiont-bearing planktic foraminifer have found that calcification rate does not typically exert a dominant control on trace element partitioning (Allen et al., 2016). Furthermore, if calcification rate were to exert a control on TE incorporation, one might expect to find higher TE compositions in calcite precipitated at higher rates, as commonly found with trace elements incorporated during inorganic calcite precipitation (e.g., Lorens, 1981; Mucci, 1988; Tesoriero and Pankow, 1996; Nehrke et al., 2007). Yet, the rapidly-precipitated gametogenic calcite exhibits consistently lower TE concentrations than the lamellar calcite among the study taxa, supporting the idea that calcification rate is unlikely to be the cause of such TE differences

throughout the chamber wall. More research is needed to better understand differences between and the motivation for these two modes of biomineralization.

Potential Vital Effects and Paleoproxy Considerations

Constraining controls on interspecies, interspecimen, and intratest trace element variability is critical to refining our understanding and utilization of foraminifera as paleoproxy substrates. The data explored herein provide insight into several considerations for foraminiferal-based paleoreconstructions. Firstly, interspecies Ba/Ca differences and variability in the range of intratest Ba/Ca chamber values lend support for the recently proposed Ba/Ca-productivity proxy in non-spinose foraminifera (Fehrenbacher et al., 2018; Fritz-Endres et al., 2022; Richey et al., 2022). In both neogloboquadrinid species we find elevated whole-test Ba/Ca and a wide range of Ba/Ca intratest values, suggesting that some of our study specimens grew under higher productivity regimes. Thus far, positive relationships between Ba/Ca and export productivity have been documented in nonspinose taxa *Neogloboquadrina dutertrei*, *Pulleniatina obliquiloculata*, and *Globorotalia truncatulinoides* (Fehrenbacher et al., 2018; Fritz-Endres et al., 2022; Richey et al., 2022). This study suggests that a similar relationship may exist in *N. incompta* and *N. pachyderma,* as well. To identify periods of high productivity in the fossil record, Ba/Ca ratios should be measured in individual specimens from each time slice of interest to examine both the interspecimen and intraspecimen (e.g., in *N. pachyderma*) variability in a population. A similar approach has been taken with examining changes in populations of individual $\delta^{18}O$ foraminiferal analyses to characterize changes El Niño intensity over time (Thirumalai et al., 2013).

Correlations between Ba/Ca and Mn/Ca (**Fig. 8**) are supportive of not only Ba as a productivity proxy, but also Mn as a potential dissolved oxygen proxy. Although research has

explored dissolved oxygen concentrations as the primary driver of Mn incorporation in benthic foraminifera, much less research has been done to identify such a relationship in planktic foraminifera (e.g., Marr et al., 2013; Davis et al., 2023). Here we show that Mn, and possibly Zn in the case of *N. pachyderma*, incorporation may be a direct result of redox conditions during calcification, and after further development could serve as critical proxies for reconstructing changes in oxygen minimum zone behavior and, when paired with Ba/Ca, particulate organic carbon flux to the seafloor.

The Na/Ca-paleosalinity proxy was recently proposed, and while field-based and culturing studies have produced promising results (Mezger et al., 2016; Bertlich et al., 2018; Dämmer et al., 2020; Bertlich et al., 2021), others are skeptical of the applicability of this ratio as a salinity proxy in deep time (Zhou et al., 2021; Gray et al., 2023). Although the data provided herein cannot settle this debate, these data contribute to fill the large data-gap in quantifying the Na/Ca composition of different planktic foraminiferal species collected from their natural living environment. Whole-test Na/Ca averages of our three study taxa ranged from approximately 10.7 to 41.7 mmol/mol (mean = 15.0 mmol/mol) for *N. incompta*, 11.3 to 25.1 mmol/mol (mean = 17.3 mmol/mol) for *N. pachyderma*, and 14.5 to 93.1 mmol/mol (mean = 24.3 mmol/mol) for *T. quinqueloba* (**Table 1**). These values are consistent with those that have been previously published on *N. pachyderma* from the Northern California Current region (Hupp and Fehrenbacher, 2023), but are higher than values reported from *N. pachyderma* collected from the Weddell Sea that were subsequently grown in culture (Bertlich et al., 2021). To our knowledge, these are the first Na/Ca ratios acquired from *N. incompta* and *T. quinqueloba* collected from plankton tows. In general, all published values of *N. pachyderma* are higher than those found in tropical spinose species (e.g., *T. sacculifer*, *G. ruber*; Mezger et al., 2016; Bertlich et al., 2018), suggesting that interspecies Na/Ca differences and Na

incorporation mechanisms are far from being understood. It is possible that elevated Na/Ca is associated with storage in NaOH-buffered preservatives (i.e., formalin) or exposure to NaOH-buffered solutions during the pre-analysis chemical cleaning procedure. However, Na/Ca data shown herein is consistent with that previously published by Hupp and Fehrenbacher (2023), in which all specimens were collected from "fresh" tows and were not exposed to preservatives. A constrained cleaning study is needed to determine the potential impact of using NaOH-buffered cleaning solutions and preservatives on individual specimens analyzed by laser ablation or solution-based ICP-MS. Regardless of this potential source of bias, we are confident in the relative differences found between species, between specimens, and within individual tests.

Contrasts in interspecies TE composition described herein appear to reflect differences in preferred habitat and therefore variation in calcification conditions. However, it is worth noting that interspecies differences are also in part controlled by the relative number of specimens collected from variable environmental regimes. Furthermore, it is recognized that individual species of foraminifera often require species-specific TE-environmental calibrations when developing paleoproxies; this is because each taxon may have different sensitivities to environmental conditions or variable approaches to calcification that produce taxon-specific partition coefficients. We can already identify some evidence of different sensitivities to trace element incorporation from the data presented herein. For example, *T. quinqueloba* does not exhibit covariance between many of the trace elements examined on the whole-test or individual chamber scale (**Fig. 8C, F**), suggesting that either 1) their trace element incorporation is less sensitive to calcifying under high productivity, low oxygen, or variable carbonate chemistry conditions and/or 2) their preferred habitat is relatively homogenous in these environmental conditions (aside from changes in temperature and salinity). We also find that *N. pachyderma*

686 shows a distinct Zn enrichment and strong positive correlation between Mn and Zn that is not
687 found in either of the other study taxa (**Fig. 2, 8**), showing further taxon-specific patterns in trace
688 element incorporation.

689 Herein we characterize the amount of chamber-to-chamber and general intratest variability
690 with the aim of identifying vital effects that could influence the appropriateness of these polar to
691 subpolar taxa for paleoreconstruction purposes. Chamber-to-chamber measurements show that on
692 average individual chamber Mg/Ca only varies from the test average by <0.5 mmol/mol across the
693 three study taxa (**Fig. 3**) with intratest ranges being < 1 mmol/mol for the neogloboquadrinids and
694 < 2 mmol/mol for *T. quinqueloba* (**Fig. 5B**). Published calibrations for *N. pachyderma* and *N.*
695 *incompta* (Davis et al., 2017) suggest that intratest variability of 1 mmol/mol would equate to a
696 few degrees C depending on the location along the logarithmic Mg/Ca-temperature calibration
697 curve. A Mg/Ca-temperature relationship has not been determined for *T. quinqueloba*.
698 Measurements of Na/Ca indicate chamber measurements vary by < 1 mmol/mol across the three
699 study taxa (**Fig. 3**) when compared to the test average and intratest ranges are found to be < 4
700 mmol/mol for the neogloboquadrinids and < 10 mmol/mol for *T. quinqueloba* (**Fig. 5C**). Published
701 Na/Ca-salinity calibrations are relatively limited and thus a difference of 1 to 10 mmol/mol could
702 equate to a change of 2 to >10 psu. Strong species-specific (e.g., Bertlich et al., 2021) and
703 instrument-specific (e.g., Gray et al., 2023) differences in Na/Ca make it difficult to constrain the
704 impact of intratest differences in Na/Ca on paleoreconstructions at this time; however, further work
705 illuminating the caveats of the proposed Na/Ca-salinity proxy will help to place these intratest
706 differences into context in regards to their potential effect on salinity reconstructions. In general,
707 intratest variability in Mg/Ca and Na/Ca is found to be greatest in *T. quinqueloba* of our three
708 study taxa. Minimal intratest variability is found in Sr/Ca (<0.05 mmol/mol comparing chambers

709 to test average; ~1 mmol/mol intratest range) among the three study taxa (**Fig. 3, 5D**), and with
710 the dominant control on Sr/Ca remaining elusive, we do not pinpoint a need for concern of
711 ontogenetic influences on paleoreconstruction at this time.

712 When comparing chamber values to the test average for Ba/Ca, we find variability of < 2
713 μmol/mol (**Fig. 4**), and intratest ranges among all chambers in the outer whorl of < 5 μmol/mol
714 (**Fig. 5E**). While Ba/Ca-export productivity calibrations have not been published for the study
715 taxa, published calibrations of *Neogloboquadrina dutertrei* and *Pulleniatina obliquiloculata*
716 suggest that differences of 2 μmol/mol would result in a change of interpreted export productivity
717 by ~0.5 mol C/m^2/yr and a difference of 5 μmol/mol could further offset export productivity
718 estimates by up to approximately 2 mol C/m^2/yr (Fritz-Endres et al., 2022). Individual chamber
719 comparisons to test averages for Mn/Ca show offsets of < 3 μmol/mol (**Fig. 4**) and intratest
720 chamber ranges of < 7 μmol/mol (**Fig. 5F**). Similar to Ba/Ca, calibrations between Mn/Ca and
721 dissolved oxygen have not been published for these taxa. However, published calibrations between
722 Mn/Ca and dissolved oxygen measured from the oxygen minimum zone-dwelling foraminifer
723 *Globorotaloides hexagonus* indicate that intratest differences of this magnitude would likely have
724 very little impact on dissolved oxygen reconstructions (Davis et al., 2023). Furthermore, studies
725 linking Mn/Ca to upwelling variability found differences in Mn/Ca for specimens of *Globigerina*
726 *ruber* (pink), *Orbulina universa*, and *Globorotalia menardii* grown during non-upwelling and
727 upwelling times to be > 10 μmol/mol on average (Davis et al., 2020). This further suggests that
728 intratest Mn/Ca found in the three study taxa herein are unlikely to obscure primary environmental
729 signals interpreted from whole-test values. As discussed, the primary control on Zn/Ca is
730 ambiguous. Individual chamber values of Zn/Ca vary by <100 μmol/mol when compared to the
731 test average (**Fig. 4**). However, the intratest range of Zn/Ca values can reach concentrations up to

nearly 400 µmol/mol. As our understanding of the primary controls of Zn/Ca evolves, so will the implications of these intratest differences in the three study taxa.

The magnitude of intratest variability described above could have impacts on Mg/Ca-temperature reconstructions, particularly for *T. quinqueloba*. Vital effects in the form of intratest differences could also impact Na/Ca-salinity reconstructions and Ba/Ca-export productivity reconstructions, though much more work is needed to refine our understanding of these potential proxies, particularly in the three taxa examined in this study. While the degree of intratest variability may be alarming, it is important to recognize that the depth habitat of an individual is not stagnant through ontogeny. Observations of population dynamics as a means to investigate reproductive strategies of planktic foraminifera living in the Red Sea have shown that individuals often deviate from a consistent depth habitat and that the depth habitat of a foraminifer changes throughout its lifetime (Meilland et al., 2021). However, statistically robust investigations of test populations show that the population, and thus the chemistry of their tests, will largely represent a consistent change in depth habitat during ontogeny. Therefore, intratest variability, such as that characterized in this study, is likely largely reflective of changes in habitat conditions or depth during an individuals' lifetime.

The data provided herein also lead to suggestions on how to approach LA-ICP-MS trace element analyses for the study taxa. Here we find that intratest trace element variability increases in tests with higher whole-test trace element values (**Table 2**). This pattern is observed as a moderate to strong positive relationship in all three taxa for most elements, aside from Sr/Ca. Therefore, when analyzing tests via LA-ICP-MS, it is imperative to conduct individual spot analyses in *all* chambers in the final whorl to determine your test average signal and not restrict

your analyses to the ultimate or penultimate chambers. Measuring all chambers in the final whorl will also allow for more direct comparison to solution-based data (Fehrenbacher et al., 2020).

Lastly, we have shown that for our three study taxa, there are predictable intrachamber differences where early ontogenetic calcite records higher trace element compositions than the gametogenic crust for nearly all trace elements (**Fig. 7**). Differences in trace element geochemistry between lamellar calcite and crust calcite are most apparent in the Mg/Ca and Na/Ca of all three taxa, as well as in the Ba/Ca composition of the neogloboquadrinids and the Zn/Ca composition of *T. quinqueloba* (**Fig. 7**). This observation has implications for how TE-environmental calibrations are constructed and how we analyze fossil specimens. For example, TE-environmental calibrations are often established from controlled culture experiments. However, tests grown in culture do not often develop a thick gametogenic crust (Davis et al., 2017; Fehrenbacher et al., 2017). We therefore echo the importance of following the recommendations and considerations brought forth by Davis et al. (2017) and Hupp and Fehrenbacher (2023), where either 1) calibrations linking TE composition to environmental variables must be established from only crusted specimens, to allow for a more direct comparison to the fossil record which is dominated by crusted specimens (Caron et al., 1990; Johnstone et al., 2010); or 2) test measurements for paleoreconstructions should use LA-ICP-MS to measure and isolate the trace element signature of the early ontogenetic calcite which more accurately records signals from the foraminifers living environment.

CONCLUSIONS

776 Here we explore interspecies, chamber-to-chamber, and intrachamber trace element
777 variability in three subpolar to polar planktic foraminiferal taxa: *Neogloboquadrina incompta*, *N.*
778 *pachyderma*, and *Turborotalita quinqueloba*. By examining large populations of thickly-calcified
779 tests (i.e., dead upon collection) collected under a wide range of environmental conditions
780 throughout the dynamic Northern California Current region, we investigate environmental versus
781 biological controls on trace element incorporation. The three study taxa show distinctly different
782 whole-test trace element values that are largely reflective of preferred living habitat. The whole-
783 test Mg/Ca and Sr/Ca ratios are highest in *T. quinqueloba* and lowest in *N. incompta*, representing
784 the shallowest and deepest depth habitats among the study taxa, respectively (**Fig. 2**).
785 *Turborotalita quinqueloba* also exhibits wide distributions of whole-test averages and intratest
786 ranges for Mg/Ca and Na/Ca, reflective of a shallow living depth with higher temperature and
787 salinity variability over an individual's ontogeny (**Figs. 2, 5**). Whole-test and individual chamber
788 Mg/Ca and Na/Ca compositions positively covary in all three study taxa further supporting their
789 incorporation mechanisms being tied to living depth habitat. The neogloboquadrinids exhibit
790 elevated Ba/Ca and Mn/Ca, and strong positive covariance between these TEs compared to *T.*
791 *quinqueloba*, indicating that some individuals calcified in an oxygen-depleted marine snow
792 microhabitat, likely during periods of elevated export production (**Figs. 2, 5, 8**). These
793 observations provide support for using the Ba/Ca of these non-spinose foraminifers as a
794 paleoproductivity proxy and potentially Mn as a paleoredox proxy. Furthermore, strong
795 correlations are found between Mn/Ca and Zn/Ca in *N. pachyderma*, suggesting that this species
796 may be able to calcify more readily under variable redox conditions than the other study taxa in
797 which hypoxic versus anoxic conditions allow for greater incorporation of Mn and Zn, respectively
798 (**Fig. 8E**). Tests with higher whole-test trace element values tend to have greater intratest trace

element variability (**Table 2**) and the outer chamber walls composed of dominantly gametogenic crust, consistently record lower trace element compositions than the lamellar calcite of the inner chamber wall formed throughout most of a foraminifers ontogeny; this pattern was found for nearly all trace elements in all three study taxa (**Fig. 7**). Intratest chamber-to-chamber variability can be quite high (**Figs. 3 – 5**), and thus laser-ablation ICP-MS studies of planktic foraminifera should always measure spot analyses of every chamber in the outer whorl. Lastly, results provide insight into the intratest trace element variability in subpolar and polar planktic foraminifera, and vast amounts of data to better understand controls on trace element incorporation in these understudied high-latitude taxa.

ACKNOWLEDGEMENTS

This work was supported by an NSF OCE grant 2222365 to B.H. and J.F. and NSF OCE 2049143 to J.F. This research was further supported by the NOAA Climate and Global Change Postdoctoral Fellowship Program to B.H., administered by UCAR's Cooperative Programs for the Advancement of Earth System Science (CPAESS) under award #NA21OAR4310383. Special thanks to J. Fisher for assistance in accessing archived tow samples and the staff at the Oregon State University Keck Collaboratory for Plasma Spectrometry.

REFERENCES

821 Alldredge, A. L., and Cohen, Y., 1987, Can microscale chemical patches persist in the sea?
822 Microelectrode Study of Marine Snow, Fecal Pellets: Science, v. 235, p. 689–691, doi:
823 10.1126/science.235.4789.689.
824 Allen, K. A., Hönisch, B., Eggins, S. M., Haynes, L. L., Rosenthal, Y., and Yu, J., 2016, Trace
825 element proxies for surface ocean conditions: A synthesis of culture calibrations with
826 planktic foraminifera: Geochimica et Cosmochimica Acta, v. 193, p. 197–221, doi:
827 10.1016/j.gca.2016.08.015.
828 Anand, P., Elderfield, H., and Conte, M. H., 2003, Calibration of Mg/Ca thermometry in
829 planktonic foraminifera from a sediment trap time series: Paleoceanography, v. 18, p.
830 2002PA000846, doi: 10.1029/2002PA000846.
831 Ariwaka, R., 1983, Distribution and taxonomy of Globigerina pachyderma (Ehrenber) off the
832 Sanriku Coast, Northeast Honshu, Japan: Tohoku University Scientific Reports, v. 53, p.
833 103-157.
834 Barth, J. A., and Wheeler, P. A., 2005, Introduction to special section: Coastal Advances in Shelf
835 Transport: Journal of Geophysical Research: Oceans, v. 110, p. 2005JC003124, doi:
836 10.1029/2005JC003124.
837 Bauch, D., Erlenkeuser, H., Winckler, G., Pavlova, G., and Thiede, J., 2002, Carbon isotopes and
838 habitat of polar planktic foraminifera in the Okhotsk Sea: the “carbonate ion effect” under
839 natural conditions: Marine Micropaleontology, v. 45, p. 83-99.
840 Bé A. W. H., and Lott, L., 1964, Shell growth and structure of planktonic foraminifera: Science,
841 v. 145, p. 823–824, doi:

842 Bé, A. W. H., 1980, Gametogenic calcification in a spinose planktonic foraminifer,
843 *Globigerinoides sacculifer* (Brady): Marine Micropaleontology, v. 5, p. 283–310, doi:
844 10.1016/0377-8398(80)90014-6.
845 Bertlich, J., Nürnberg, D., Hathorne, E. C., de Nooijer, L. J., Mezger, E. M., Kienast, M.,
846 Nordhausen, S., Reichart, G.-J., Schönfeld, J., and Bijma, J., 2018, Salinity control on Na
847 incorporation into calcite tests of the planktonic foraminifera *Trilobatus sacculifer* –
848 evidence from culture experiments and surface sediments: Biogeosciences, v. 15, p. 5991–
849 6018, doi: 10.5194/bg-15-5991-2018.
850 Bertlich, J., Gussone, N., Berndt, J., Arlinghaus, H. F., and Dieckmann, G. S., 2021, Salinity
851 effects on cultured *Neogloboquadrina pachyderma* (sinistral) from high latitudes: new
852 paleoenvironmental insights: Geo-Marine Letters, v. 41, p. 2, doi: 10.1007/s00367-020-
853 00677-1.
854 Billups, K., Rickaby, R.E.M., and Schrag, D.P., 2004, Cenozoic pelagic Sr/Ca records:
855 Exploring a link to paleoproductivity: Paleoceanography, v. 19, p. PA3005,
856 doi:10.1029/2004PA001011.
857 Bolton, A., 2011, LA-ICP-MS Trace Element Analysis of Planktonic Foraminifera and
858 Application to Marine Isotope Stage 31 in the Southwest Pacific Ocean. Thesis.
859 Bolton, A., and Marr, J. P., 2013, Trace element variability in crust-bearing and non crust-
860 bearing *Neogloboquadrina incompta*, P–D intergrade and *Globoconella inflata* from the
861 Southwest Pacific Ocean: Potential paleoceanographic implications: Marine
862 Micropaleontology, v. 100, p. 21–33, doi: 10.1016/j.marmicro.2013.03.008.

Bonnin, E. A., Zhu, Z., Fehrenbacher, J. S., Russell, A. D., Hönisch, B., Spero, H. J., and Gagnon, A. C., 2019, Submicron sodium banding in cultured planktic foraminifera shells: Geochimica et Cosmochimica Acta, v. 253, p. 127–141, doi: 10.1016/j.gca.2019.03.024.

Boussetta, S., Bassinot, F., Sabbatini, A., Caillon, N., Nouet, J., Kallel, N., Rebaubier, H., Klinkhammer, G., and Labeyrie, L., 2011, Diagenetic Mg-rich calcite in Mediterranean sediments: Quantification and impact on foraminiferal Mg/Ca thermometry: Marine Geology, v. 280, p. 195-204.

Branson, O., Read, E., Redfern, S. A. T., Rau, C., and Elderfield, H., 2015, Revisiting diagenesis on the Ontong Java Plateau: Evidence for authigenic crust precipitation in *Globorotalia tumida*: Paleoceanography, v. 30, p. 1490–1502, doi: 10.1002/2014PA002759.

Branson, O., Fehrenbacher, J. S., Vetter, L., Sadekov, A. Y., Eggins, S. M., and Spero, H. J., 2019, LAtools: A data analysis package for the reproducible reduction of LA-ICPMS data: Chemical Geology, v. 504, p. 83–95, doi: 10.1016/j.chemgeo.2018.10.029.

Bryan, S. P., and Marchitto, T. M., 2010, Testing the utility of paleonutrient proxies Cd/Ca and Zn/Ca in benthic foraminifera from thermocline waters: Geochemistry, Geophysics, Geosystems, v. 11, p. 2009GC002780, doi: 10.1029/2009GC002780.

Caron, D. A., Roger Anderson, O., Lindsey, J. L., Faber, W. W., and Lin Lim, E. E., 1990, Effects of gametogenesis on test structure and dissolution of some spinose planktonic foraminifera and implications for test preservation: Marine Micropaleontology, v. 16, p. 93–116, doi: 10.1016/0377-8398(90)90031-G.

Carter, S. C., Paytan, A., and Griffith, E. M., 2020, Toward an improved understanding of the marine barium cycle and the application of marine barite as a paleoproductivity proxy: Minerals, v. 10, p. 421, doi: 10.3390/min10050421.

886 Dämmer, L. K., de Nooijer, L., Van Sebille, E., Haak, J. G., and Reichart, G.-J., 2020,
887 Evaluation of oxygen isotopes and trace elements in planktonic foraminifera from the
888 Mediterranean Sea as recorders of seawater oxygen isotopes and salinity: Climate of the
889 Past, v. 16, p. 2401–2414, doi: 10.5194/cp-16-2401-2020.
890 Davis, C. V., Fehrenbacher, J. S., Hill, T. M., Russell, A. D., and Spero, H. J., 2017,
891 Relationships between temperature, pH, and crusting on Mg/Ca ratios in laboratory-grown
892 *Neogloboquadrina* foraminifera: Paleoceanography, v. 32, p. 1137–1152, doi:
893 10.1002/2017PA003111.
894 Davis, C. V., Fehrenbacher, J. S., Benitez-Nelson, C., and Thunell, R. C., 2020, Trace element
895 heterogeneity across individual planktic foraminifera from the modern Cariaco Basin:
896 Journal of Foraminiferal Research, v. 50, p. 204–218, doi: 10.2113/gsjfr.50.2.204.
897 Davis, C. V., Doherty, S., Fehrenbacher, J., and Wishner, K., 2023, Trace element composition
898 of modern planktic foraminifera from an oxygen minimum zone: Potential proxies for an
899 enigmatic environment: Frontiers in Marine Science, v. 10, p. 1145756, doi:
900 10.3389/fmars.2023.1145756.
901 de Nooijer, L. J., Spero, H. J., Erez, J., Bijma, J., and Reichart, G. J., 2014, Biomineralization in
902 perforate foraminifera: Earth-Science Reviews, v. 135, p. 48–58, doi:
903 10.1016/j.earscirev.2014.03.013.
904 de Nooijer, L. J., Brombacher, A., Mewes, A., Langer, G., Nehrke, G., Bijma, J., and Reichart,
905 G.-J., 2017, Ba incorporation in benthic foraminifera: Biogeochemistry: Biomineralization,
906 accessed February 27, 2024, at https://bg.copernicus.org/preprints/bg-2017-45/bg-2017-
907 45.pdf.

908 Dymond, J., and Collier, R.,1996, Particulate barium fluxes and their relationships to biological
909 productivity: Deep Sea Research Part II: Topical Studies in Oceanography, v. *43*, p. 1283–
910 1308, doi: 10.1016/0967-0645(96)00011-2
911 Edgar, K.M., Anagnostou, E., Pearson, P.N., and Foster, G.L., 2015, Assessing the impact of
912 diagenesis on $\delta^{11}B$, $\delta^{13}C$, $\delta^{18}O$, Sr/Ca and B/Ca values in fossil planktic foraminiferal
913 calcite: Geochimica et Cosmochimica Acta, v. 166, p. 189-209.
914 Eggins, S., De Deckker, P., and Marshall, J., 2003, Mg/Ca variation in planktonic foraminifera
915 tests: implications for reconstructing palaeo-seawater temperature and habitat migration:
916 Earth and Planetary Science Letters, v. 212, p. 291–306, doi: 10.1016/S0012-
917 821X(03)00283-8.
918 Erez, J., 2003, The source of ions for biomineralization in foraminifera and their implications for
919 paleoceanographic proxies: Reviews in mineralogy and geochemistry, v. 54, p. 115-149,
920 doi: 10.2113/0540115
921 Evans, D., Müller, W., and Erez, J., 2018, Assessing foraminifera biomineralization models
922 through trace element data of cultures under variable seawater chemistry: Geochimica et
923 Cosmochimica Acta, v. 236, p. 198-217.
924 Fehrenbacher, J. S., Russell, A. D., Davis, C. V., Gagnon, A. C., Spero, H. J., Cliff, J. B., Zhu,
925 Z., and Martin, P., 2017, Link between light-triggered Mg-banding and chamber formation
926 in the planktic foraminifera *Neogloboquadrina dutertrei*: Nature Communications, v. 8, p.
927 15441, doi: 10.1038/ncomms15441.
928 Fehrenbacher, J. S., Russell, A. D., Davis, C. V., Spero, H. J., Chu, E., and Hönisch, B., 2018,
929 Ba/Ca ratios in the non-spinose planktic foraminifer *Neogloboquadrina dutertrei*: Evidence

for an organic aggregate microhabitat: Geochimica et Cosmochimica Acta, v. 236, p. 361–372, doi: 10.1016/j.gca.2018.03.008.

Fehrenbacher, J., Marchitto, T., and Spero, H. J., 2020, Comparison of laser ablation and solution-based ICP-MS results for individual foraminifer Mg/Ca and Sr/Ca analyses: Geochemistry, Geophysics, Geosystems, v. 21, p. e2020GC009254, doi: 10.1029/2020GC009254.

Feinberg, L. R., and Peterson, W. T., 2003, Variability in duration and intensity of euphausiid spawning off central Oregon, 1996–2001: Progress in Oceanography, v. 57, p. 363–379, doi: 10.1016/S0079-6611(03)00106-X.

Fritz-Endres, T., Fehrenbacher, J. S., Russell, A. D., and Cynar, H., 2022, Increased productivity in the equatorial Pacific during the deglaciation inferred from the Ba/Ca ratios of non-spinose planktic foraminifera: Paleoceanography and Paleoclimatology, v. 37, p. e2022PA004506, doi: 10.1029/2022PA004506.

Gray, W. R., Evans, D., Henehan, M., Weldeab, S., Lea, D. W., Müller, W., and Rosenthal, Y., 2023, Sodium incorporation in foraminiferal calcite: An evaluation of the Na/Ca salinity proxy and evidence for multiple Na-bearing phases: Geochimica et Cosmochimica Acta, v. 348, p. 152–164, doi: 10.1016/j.gca.2023.03.011.

Greco, M., Jonkers, L., Kretschmer, K., Bijma, J., and Kucera, M., 2019, Depth habitat of the planktonic foraminifera *Neogloboquadrina pachyderma* in the northern high latitudes explained by sea-ice and chlorophyll concentrations: Biogeosciences, v. 16, p. 3425–3437, doi: 10.5194/bg-16-3425-2019.

951 Griffith, E. M., and Paytan, A., 2012, Barite in the ocean – occurrence, geochemistry and
952 palaeoceanographic applications: Sedimentology, v. 59, p. 1817–1835, doi: 10.1111/j.1365-
953 3091.2012.01327.x.
954 Hathorne, E. C., Alard, O., James, R. H., and Rogers, N. W., 2003, Determination of intratest
955 variability of trace elements in foraminifera by laser ablation inductively coupled plasma-
956 mass spectrometry: Geochemistry, Geophysics, Geosystems, v. 4, p. 2003GC000539, doi:
957 10.1029/2003GC000539.
958 Hathorne, E. C., James, R. H., and Lampitt, R. S., 2009, Environmental versus biomineralization
959 controls on the intratest variation in the trace element composition of the planktonic
960 foraminifera *G. inflata* and *G. scitula*: Paleoceanography, v. 24, p. 2009PA001742, doi:
961 10.1029/2009PA001742.
962 Holland, K., Branson, O., Haynes, L. L., Hönisch, B., Allen, K. A., Russell, A. D., Fehrenbacher,
963 J. S., Spero, H. J., and Eggins, S. M., 2020, Constraining multiple controls on planktic
964 foraminifera Mg/Ca: Geochimica et Cosmochimica Acta, v. 273, p. 116–136, doi:
965 10.1016/j.gca.2020.01.015.
966 Hönisch, B., Allen, K. A., Russell, A. D., Eggins, S. M., Bijma, J., Spero, H. J., Lea, D. W., and
967 Yu, J., 2011, Planktic foraminifers as recorders of seawater Ba/Ca: Marine
968 Micropaleontology, v. 79, p. 52–57, doi: 10.1016/j.marmicro.2011.01.003.
969 Hönisch, B., Allen, K. A., Lea, D. W., Spero, H. J., Eggins, S. M., Arbuszewski, J., deMenocal,
970 P., Rosenthal, Y., Russell, A. D., and Elderfield, H., 2013, The influence of salinity on
971 Mg/Ca in planktic foraminifers – Evidence from cultures, core-top sediments and
972 complementary δ18O: Geochimica et Cosmochimica Acta, v. 121, p. 196–213, doi:
973 10.1016/j.gca.2013.07.028.

974 Hupp, B. N., and Fehrenbacher, J. S., 2023, Geochemical differences between alive, uncrusted
975 and dead, crusted Shells of *Neogloboquadrina pachyderma* : Implications for
976 paleoreconstruction: Paleoceanography and Paleoclimatology, v. 38, p. e2023PA004638,
977 doi: 10.1029/2023PA004638.
978 Jochum, K. P., Weis, U., Stoll, B., Kuzmin, D., Yang, Q., Raczek, I., Jacob, D. E., Stracke, A.,
979 Birbaum, K., Frick, D. A., Günther, D., and Enzweiler, J., 2011, Determination of
980 Reference Values for NIST SRM 610–617 Glasses Following ISO Guidelines:
981 Geostandards and Geoanalytical Research, v. 35, p. 397–429, doi: 10.1111/j.1751-
982 908X.2011.00120.x.
983 Johnstone, H. J. H., Schulz, M., Barker, S., and Elderfield, H., 2010, Inside story: An X-ray
984 computed tomography method for assessing dissolution in the tests of planktonic
985 foraminifera: Marine Micropaleontology, v. 77, p. 58–70, doi:
986 10.1016/j.marmicro.2010.07.004.
987 Katz, M. E., Cramer, B. S., Franzese, A., Honisch, B., Miller, K. G., Rosenthal, Y., and Wright,
988 J. D., 2010, Traditional and emerging geochemical proxies in foraminifera: The Journal of
989 Foraminiferal Research, v. 40, p. 165–192, doi: 10.2113/gsjfr.40.2.165.
990 Kirincich, A. R., Barth, J. A., Grantham, B. A., Menge, B. A., and Lubchenco, J., 2005, Wind-
991 driven inner-shelf circulation off central Oregon during summer: Journal of Geophysical
992 Research: Oceans, v. 110, p. 2004JC002611, doi: 10.1029/2004JC002611.
993 Kniskern, T. A., Warrick, J. A., Farnsworth, K. L., Wheatcroft, R. A., and Goñi, M. A., 2011,
994 Coherence of river and ocean conditions along the US West Coast during storms:
995 Continental Shelf Research, v. 31, p. 789–805, doi: 10.1016/j.csr.2011.01.012.

Kozdon, R., Kelly, D.C., Kitajima, K., Strickland, A., Fournelle, J.H., and Valley, J.W., 2013, *In situ* $\delta^{18}O$ and Mg/Ca analyses of diagenetic and planktic foraminiferal calcite preserved in a deep-sea record of the Paleocene-Eocene thermal maximum: Paleoceanography, v. 28, p. 1-12, doi:10.1002/palo.20048

Lane, M. K., Fehrenbacher, J. S., Fisher, J. L., Fewings, M. R., Crump, B. C., Risien, C. M., Meyer, G. M. L., and Schell, F., 2023, Planktonic foraminiferal assemblages reflect warming during two recent mid-latitude marine heatwaves: Frontiers in Marine Science, v. 10, p. 1155761, doi: 10.3389/fmars.2023.1155761.

Lea, D. W., Mashiotta, T. A., and Spero, H. J., 1999, Controls on magnesium and strontium uptake in planktonic foraminifera determined by live culturing: Geochimica et Cosmochimica Acta, v. 63, p. 2369–2379, doi: 10.1016/S0016-7037(99)00197-0.

Lebrato M., et al., 2020, Global variability in seawater Mg:Ca and Sr:Ca ratios in the modern ocean: Proceedings of the National Academy of Sciences, v. 117, 22281-22292, doi: 10.1073/pnas.1918943117.

Longerich, H. P., Jackson, S. E., and Günther, D., 1996. Inter-laboratory note. Laser ablation inductively coupled plasma mass spectrometric transient signal data acquisition and analyte concentration calculation: Journal of Analytical Atomic Spectrometry, v. 1, p. 899–904, doi: 10.1039/ja9961100899

Lorens, 1981, Sr, Cd, Mn and Co distribution coefficients in calcite as a function of calcite precipitation rate: Geochimica et Cosmochimica Acta, v. 45, p. 553-561, doi: 10.1016/0016-7037(81)90188-5.

1017 Marchitto, T. M., Curry, W. B., and Oppo, D. W., 2000, Zinc concentrations in benthic
1018 foraminifera reflect seawater chemistry: Paleoceanography, v. 15, p. 299–306, doi:
1019 10.1029/1999PA000420.
1020 Marr, J. P., Carter, L., Bostock, H. C., Bolton, A., and Smith, E., 2013, Southwest Pacific Ocean
1021 response to a warming world: Using Mg/Ca, Zn/Ca, and Mn/Ca in foraminifera to track
1022 surface ocean water masses during the last deglaciation: Paleoceanography, v. 28, p. 347–
1023 362, doi: 10.1002/palo.20032.
1024 Martínez-Botí, M. A., Mortyn, P. G., Schmidt, D. N., Vance, D., and Field, D. B., 2011, Mg/Ca
1025 in foraminifera from plankton tows: Evaluation of proxy controls and comparison with core
1026 tops: Earth and Planetary Science Letters, v. 307, p. 113–125, doi:
1027 10.1016/j.epsl.2011.04.019.
1028 Martinez-Ruiz, F., Paytan, A., Gonzalez-Muñoz, M. T., Jroundi, F., Abad, M. M., Lam, P. J.,
1029 Bishop, J. K. B., Horner, T. J., Morton, P. L., and Kastner, M., 2019, Barite formation in the
1030 ocean: Origin of amorphous and crystalline precipitates: Chemical Geology, v. 511, p. 441–
1031 451, doi: 10.1016/j.chemgeo.2018.09.011.
1032 Martinez-Ruiz, F., Paytan, A., Gonzalez-Muñoz, M. T., Jroundi, F., Abad, M. M., Lam, P. J.,
1033 Horner, T. J., and Kastner, M., 2020, Barite precipitation on suspended organic matter in the
1034 mesopelagic zone: Frontiers in Earth Science, v. 8, p. 567714, doi:
1035 10.3389/feart.2020.567714.
1036 Mashiotta, T. A., Lea, D. W., and Spero, H. J., 1999, Glacial–interglacial changes in
1037 Subantarctic sea surface temperature and δ^{18}O-water using foraminiferal Mg: Earth and
1038 Planetary Science Letters, v. 170, p. 417–432, doi: 10.1016/S0012-821X(99)00116-8.

1039 Meilland, J., Siccha, M., Kaffenberger, M., Bijma, J., and Kucera, M., 2021, Population
1040 dynamics and reproduction strategies of planktonic foraminifera in the open ocean:
1041 Biogeosciences, v. 18, p. 5789–5809, doi: 10.5194/bg-18-5789-2021.
1042 Mezger, E. M., de Nooijer, L. J., Boer, W., Brummer, G. J. A., and Reichart, G. J., 2016, Salinity
1043 controls on Na incorporation in Red Sea planktonic foraminifera: Paleoceanography, v. 31,
1044 p. 1562–1582, doi: 10.1002/2016PA003052.
1045 Mezger, E.M., de Nooijer, L.J., Siccha, M., Brummer, G.J.A., Kucera, M., and Reichart, G.J.,
1046 2018, Taphonomic and ontogenetic effects on Na/Ca and Mg/Ca in spinose planktonic
1047 foraminifera from the Red Sea: Geochemistry, Geophysics, Geosystems, v. 19, p. 4174-
1048 4194, doi: 10.1029/2018GC007852.
1049 Mucci, A., 1988, Manganese uptake during calcite precipitation from seawater: conditions
1050 leading to the formation of a pseudokutnahorite: Geochimica et Cosmochimica Acta, v. 52,
1051 p. 1859-1868.
1052 Mulitza, S., Dürkoop, A., Hale, W., Wefer, G., and Stefan Niebler, H., 1997, Planktonic
1053 foraminifera as recorders of past surface-water stratification: Geology, v. 25, p. 335, doi:
1054 10.1130/0091-7613(1997)025<0335:PFAROP>2.3.CO;2.
1055 Nehrke, G., Reichart, G.J., Van Cappellen, P., Meile, C., and Bijma, J., 2007, Dependence of
1056 calcite growth rate and Sr partitioning on solution stoichiometry: Geochimica et
1057 Cosmochimica Acta, v. 71, p. 2240-2249.
1058 Niebler, H. S., Hubberten, H. W., and Gersonde, R. (1999). Oxygen isotope values of planktic
1059 foraminifera: A tool for the reconstruction of surface water stratification. *In* G. Fischer, and
1060 G. Wefer (eds.), Use of proxies in Paleoceanography: Examples from the South Atlantic
1061 (pp. 165–189). Springer.

1062 Nürnberg, D., 1995, Magnesium in tests of Neogloboquadrina pachyderma sinistral from high
1063 northern and southern latitudes: Journal of Foraminiferal Research, v. 25, p. 350-368.
1064 Nürnberg, D., Bijma, J., and Hemleben, C., 1996, Assessing the reliability of magnesium in
1065 foraminiferal calcite as a proxy for water mass temperatures: Geochimica et Cosmochimica
1066 Acta, v. 60, p. 803-814.
1067 Ortiz, J. D., and Mix, A. C., 1992, The spatial distribution and seasonal succession of planktonic
1068 foraminifera in the California Current off Oregon, September 1987 – September 1988:
1069 Geological Society, London, Special Publications, v. 64, p. 197–213, doi:
1070 10.1144/GSL.SP.1992.064.01.13.
1071 Ortiz, J.D., Mix, A.C., Rugh, W., Watkins, J.M., and Collier, R.W., 1996, Deep-dwelling
1072 planktonic foraminifera of the northeastern Pacific Ocean reveal environmental control of
1073 oxygen and carbon isotopic disequilibria: Geochimica et Cosmochimica Acta, v. 60, p.
1074 4509-4523.
1075 Paulmier, A., and Ruiz-Pino, D., 2009, Oxygen minimum zones (OMZs) in the modern ocean:
1076 Progress in Oceanography, v. 80, p. 113–128, doi: 10.1016/j.pocean.2008.08.001.
1077 Pearson, P.N., and Kucera, M., 2018, Chapter 12: Taxonomy, biostratigraphy, and phylogeny of
1078 Oligocene Turborotalita *in* Wade, B.S., Olsson, R.K., Pearson, P.N., Huber, B.T., and
1079 Berggren, W.A. (eds.), 2018, Atlas of Oligocene Planktonic Foraminifera: Cushman
1080 Foundation for Foraminiferal Research Volume 46
1081 Perlin, A., Moum, J. N., Klymak, J. M., Levine, M. D., Boyd, T., and Kosro, P. M., 2005, A
1082 modified law-of-the-wall applied to oceanic bottom boundary layers: Journal of
1083 Geophysical Research: Oceans, v. 110, p. 2004JC002310, doi: 10.1029/2004JC002310.

1084 Pierce, S. D., Barth, J. A., Shearman, R. K., and Erofeev, A. Y., 2012, Declining Oxygen in the
1085 Northeast Pacific: Journal of Physical Oceanography, v. 42, p. 495–501, doi: 10.1175/JPO-
1086 D-11-0170.1.
1087 Rebotim, A., Voelker, A.H.L., Jonkers, L., Waniek, J.J., Meggers, H., Schiebel, R., Fraile, I.,
1088 Schulz, M., and Kucera, M., 2017, Factors controlling the depth habitat of planktonic
1089 foraminifera in the subtropical eastern North Atlantic: Biogeosciences, v. 14, p. 827-859,
1090 doi:10.5194/bg-14-827-2017.
1091 Richey, J. N., Fehrenbacher, J. S., Reynolds, C. E., Davis, C. V., and Spero, H. J., 2022, Barium
1092 enrichment in the non-spinose planktic foraminifer, *Globorotalia truncatulinoides*:
1093 Geochimica et Cosmochimica Acta, v. 333, p. 184–199, doi: 10.1016/j.gca.2022.07.006.
1094 Russell, A. D., Hönisch, B., Spero, H. J., and Lea, D. W., 2004, Effects of seawater carbonate
1095 ion concentration and temperature on shell U, Mg, and Sr in cultured planktonic
1096 foraminifera: Geochimica et Cosmochimica Acta, v. 68, p. 4347–4361, doi:
1097 10.1016/j.gca.2004.03.013.
1098 Sadekov, A.Y., Eggins, S.M., and De Dekker, P., 2005, Characterization of Mg/Ca distributions
1099 in planktonic foraminifera species by electron microprobe mapping: Geochemistry,
1100 Geophysics, Geosystems, v. 6, p. Q12P06, doi:10.1029/2005GC000973.
1101 Sadekov, A. Yu., Eggins, S. M., Klinkhammer, G. P., and Rosenthal, Y., 2010, Effects of
1102 seafloor and laboratory dissolution on the Mg/Ca composition of *Globigerinoides sacculifer*
1103 and *Orbulina universa* tests — A laser ablation ICPMS microanalysis perspective: Earth
1104 and Planetary Science Letters, v. 292, p. 312–324, doi: 10.1016/j.epsl.2010.01.039.
1105 Schiebel, R., and Hemleben, C., 2017, Planktic Foraminifers in the Modern Ocean: Springer
1106 Berlin Heidelberg, Berlin, Heidelberg.

Simstich, J., Sarnthein, M., and Erlenkeuser, H., 2003, Paired $\delta^{18}O$ signals of *Neogloboquadrina pachyderma* (s) and *Turborotalita quinqueloba* show thermal stratification structure in Nordic Seas: Marine Micropaleontology, v. 48, p. 107-125.

Steinhardt, J., Cléroux, C., Ullgren, J., de Nooijer, L., Durgadoo, J. V., Brummer, G.-J., and Reichart, G.-J., 2014, Anti-cyclonic eddy imprint on calcite geochemistry of several planktonic foraminiferal species in the Mozambique Channel: Marine Micropaleontology, v. 113, p. 20–33, doi: 10.1016/j.marmicro.2014.09.001.

Steinhardt, J., de Nooijer, L. L. J., Brummer, G., and Reichart, G., 2015, Profiling planktonic foraminiferal crust formation: Geochemistry, Geophysics, Geosystems, v. 16, p. 2409–2430, doi: 10.1002/2015GC005752.

Stoll H.M., Schrag, D.P., and Clemens, S.C., 1999, Are seawater Sr/Ca variations preserved in quaternary foraminifera?: Geochimica et Cosmochimica Acta, v. 63, p. 3535-3547.

Taylor, B. J., Rae, J. W. B., Gray, W. R., Darling, K. F., Burke, A., Gersonde, R., Abelmann, A., Maier, E., Esper, O., and Ziveri, P., 2018, Distribution and ecology of planktic foraminifera in the North Pacific: Implications for paleo-reconstructions: Quaternary Science Reviews, v. 191, p. 256–274, doi: 10.1016/j.quascirev.2018.05.006.

Tesoriero, A.J., and Pankow, J.F., 1996, Solid solution partitioning of Sr^{2+}, Ba^{2+}, and Cd^{2+} to calcite: Geochimica et Cosmochimica Acta, v. 60, p. 1053-1063.

Thirumalai, K., Partin, J. W., Jackson, C. S., and Quinn, T. M., 2013, Statistical constraints on El Niño Southern Oscillation reconstructions using individual foraminifera: A sensitivity analysis: Paleoceanography, v. 28, p. 401–412, doi: 10.1002/palo.20037.

van Dijk, I., de Nooijer, L. J., and Reichart, G.-J., 2017, Trends in element incorporation in hyaline and porcelaneous foraminifera as a function of pCO_2: Biogeosciences, v. 14, p. 497–510, doi: 10.5194/bg-14-497-2017.

Watkins, C. S., Schmidt, M. W., and Hertzberg, J. E., 2021, Calibrating *Trilobatus sacculifer* Na/Ca ratios from Atlantic core-tops as a proxy for sea surface salinity: Paleoceanography and Paleoclimatology, v. 36, p. e2021PA004277, doi: 10.1029/2021PA004277.

Wit, J.C., de Nooijer, L.J., Wolthers, M., and Reichart, G.J., 2013, A novel salinity proxy based on Na incorporation into foraminiferal calcite: Biogeosciences, v. 10, p. 6375-6387, doi:10.5194/bg-10-6375-2013.

Zhou, X., Rosenthal, Y., Haynes, L., Si, W., Evans, D., Huang, K.-F., Hönisch, B., and Erez, J., 2021, Planktic foraminiferal Na/Ca: A potential proxy for seawater calcium concentration: Geochimica et Cosmochimica Acta, v. 305, p. 306–322, doi: 10.1016/j.gca.2021.04.012.

CAPTIONS

Table 1. Summary statistics of the populations of whole-shell TE/Ca values including number of individuals measured, the mean, standard deviation, maximum and minimum values, the range, and inter-quartile range. Note that these values were calculated to include outliers that are not incorporated into the boxplots shown in Figure 2.

Table 2. Covariance values (r^2 and p-value) comparing the intratest range and intratest standard deviation (SD) of a given TE/Ca to the whole-test average of that same TE/Ca, evaluated for each of the study taxa. Asterisks indicate regressions where outliers were removed because they had a strong bias on the covariance results.

Table 3. Summary of systematic chamber-to-chamber differences in TE/Ca composition with the addition of each new chamber, as determined in this study and shown in Figures 3 and 4.

Figure 1. Bathymetric map of plankton tow sites (red circles) in the Northern California Current off the coast of Washington (WA), Oregon (OR), and California (CA) in the United States. The scale bar is in kilometers.

Figure 2. A) Schematic approach used to calculate the whole-test average for each individual test. B-G) Violin plots with inset boxplots showing the distribution of whole-test TE/Ca values for the study specimens belonging to the three study species (*N. incompta*, N = 92; *N. pachyderma*, N = 55; and *T. quinqueloba*, N = 42) for B) Mg/Ca, C) Na/Ca, D) Sr/Ca, E) Ba/Ca, F) Mn/Ca, and G) Zn/Ca. Foraminifer cartoon in panel A adapted from Hupp and Fehrenbacher (2023).

Figure 3. A) Schematic approach used to normalize each chamber value (mean centered) to account for growth under variable environmental conditions. The distribution normalized chamber values (e.g., $F3_{normalized}$) for each chamber and taxon is shown in the remaining panels. B-J) Violin plots with inset boxplots showing the distribution of TE/Ca averages for each

individual chamber normalized to the test average TE/Ca composition for B-D) *N. incompta*, E-G) *N. pachyderma*, and H-J) *T. quinqueloba*. Trace elements examined include Mg/Ca (panels B, E, H), Na/Ca (panels C, F, I), and Sr/Ca (panels D, G, J). F0 refers to the youngest chamber in the outer whorl, with progressively older chambers referred to as F1, F2, F3, and F4, respectively. Numbers listed below each chamber along the x-axis indicate the number of measurements contributing to the TE/Ca distributions associated with that chamber for each taxon. Note the variable y-axes between panels.

Figure 4. Violin plots with inset boxplots showing the distribution of TE/Ca averages for each individual chamber normalized to the test average TE/Ca composition for A-C) *N. incompta*, D-F) *N. pachyderma*, and G-I) *T. quinqueloba*. Trace elements examined include Ba/Ca (panels A, D, G), Mn/Ca (panels B, E, H), and Zn/Ca (panels C, F, I). F0 refers to the youngest chamber in the outer whorl, with progressively older chambers referred to as F1, F2, F3, and F4, respectively. Note that the same approach illustrated in Figure 3A was used to determine the normalized chamber values plotted in these violin plots. Numbers listed below each chamber along the x-axis indicate the number of measurements contributing to the TE/Ca distributions associated with that chamber for each taxon. Note the variable y-axes between panels.

Figure 5. A) Schematic showing a hypothetical example of how the intratest range was calculated for each individual test. The range was determined by subtracting the chamber with the lowest average from the chamber with the highest average from the same test. B-G)Violin plots with inset boxplots showing the intratest range of TE/Ca values measured in individual tests of the three study taxa (*N. incompta*, N = 92; *N. pachyderma*, N = 55; and *T. quinqueloba*,

N = 42). Trace elements examined include B) Mg/Ca, C) Na/Ca, D) Sr/Ca, E) Ba/Ca, F) Mn/Ca, and G) Zn/Ca.

Figure 6. Schematic workflow illustrating how the spectrum from a single spot measurement can be evaluated to assess intrachamber variability.

Figure 7. Comparison of averages of the inner 50% of each chamber wall spectrum to the outer 50% of the same test spectrum. The dashed line denotes the line of equality and the solid blue line represents the trendline of the data. Data is shown for A-F) *N. incompta*, G-L) *N. pachyderma*, and M-R) *T. quinqueloba*. Note the variable axes between panels.

Figure 8. Covariance matrices of whole-test average TE/Ca values (A-C) and covariance matrices comparing the average TE composition of individual chambers(D-F). Panels shown are separated by taxa for A and D) *N. incompta*, B and E) *N. pachyderma*, and C and F) *T. quinqueloba*. Boxes are colored according to the strength and sign (blue = positive correlation, red = negative correlation) of the R^2 value, consistent with the scale to the right of each matrix. Only correlations where the p-value is ≤ 0.05 are shown (i.e., blanks represent regressions where p-values were > 0.05).

Table 1.

Taxon	Statistic	Mg/Ca (mmol/mol)	Na/Ca (mmol/mol)	Sr/Ca (mmol/mol)	Ba/Ca (µmol/mol)	Mn/Ca (µmol/mol)	Zn/Ca (µmol/mol)
N. incompta (N = 92)	Mean	2.11	15.01	1.34	14.03	9.91	256.02
	Std Dev. (2σ)	2.10	6.85	0.15	38.79	17.49	445.53
	Max.	7.62	41.66	1.79	136.95	47.53	1353.77
	Min.	1.04	10.73	1.04	1.12	1.16	30.13
	Range	6.58	30.92	0.75	135.83	46.36	1323.64
	IQR	0.82	1.76	0.06	16.69	8.97	240.83
N. pachyderma (N = 55)	Mean	2.37	17.25	1.37	26.77	6.52	501.18
	Std Dev. (2σ)	1.66	5.74	0.16	152.07	15.67	641.16
	Max.	5.22	25.07	1.53	386.34	40.23	1587.37
	Min.	1.01	11.34	1.06	0.98	1.40	81.44
	Range	4.21	13.73	0.47	385.36	38.82	1505.93
	IQR	1.04	3.84	0.10	7.14	3.55	368.94
T. quinqueloba (N = 42)	Mean	2.88	24.28	1.43	10.87	8.83	370.85
	Std Dev. (2σ)	1.83	25.25	0.30	65.85	14.87	821.12
	Max.	5.32	93.07	1.55	191.91	40.77	2090.17
	Min.	1.64	14.54	0.59	1.32	2.86	93.40
	Range	3.68	78.53	0.95	190.59	37.90	1996.77
	IQR	1.17	8.45	0.07	2.54	5.15	309.79

Table 2.

TE/Ca	Intratest:	*N. incompta*		*N. pachyderma*		*T. quinqueloba*	
		r^2	p-value	r^2	p-value	r^2	p-value
Mg/Ca	Range	0.67	$2.2 \cdot 10^{-16}$	0.58	$9.1 \cdot 10^{-12}$	0.18	0.0029
	SD	0.68	$2.2 \cdot 10^{-16}$	0.58	$9.1 \cdot 10^{-12}$	0.16	0.0057
Na/Ca	Range	0.53	$2.2 \cdot 10^{-16}$	0.36	$6.7 \cdot 10^{-7}$	0.32	$5.8 \cdot 10^{-5}$
	SD	0.534	$2.2 \cdot 10^{-16}$	0.36	$8.3 \cdot 10^{-7}$	0.33	$4.1 \cdot 10^{-5}$
Sr/Ca	Range	$4.3*10^{-4}$	0.31	0.0047*	0.27	-0.022*	0.66
	SD	$7.7*10^{-4}$	0.31	0.0099*	0.23	-0.025*	0.77
Ba/Ca	Range	0.64	$2.2 \cdot 10^{-16}$	0.98	$2.2 \cdot 10^{-16}$	0.75	$6.9 \cdot 10^{-14}$
	SD	0.64	$2.2 \cdot 10^{-16}$	0.99	$2.2 \cdot 10^{-16}$	0.76	$5.4 \cdot 10^{-14}$
Mn/Ca	Range	0.70	$2.2 \cdot 10^{-16}$	0.41	$7.2 \cdot 10^{-8}$	0.77	$2.4 \cdot 10^{-14}$
	SD	0.72	$2.2 \cdot 10^{-16}$	0.39	$2.6 \cdot 10^{-7}$	0.78	$4.1 \cdot 10^{-15}$
Zn/Ca	Range	0.37	$6.6 \cdot 10^{-11}$	0.51	$5.3 \cdot 10^{-10}$	0.62	$3.3 \cdot 10^{-10}$
	SD	0.38	$3.4 \cdot 10^{-11}$	0.49	$1.6 \cdot 10^{-9}$	0.61	$7.5 \cdot 10^{-10}$

Table 3.

TE/Ca	*N. incompta*	*N. pachyderma*	*T. quinqueloba*
Mg/Ca	Decrease	Decrease	Decrease (except F4)
Na/Ca	Increase (F0 only)	--	--
Sr/Ca	Increase	Decrease	--
Ba/Ca	--	Decrease	Decrease
Mn/Ca	--	Decrease	Decrease
Zn/Ca	Increase	Increase	Decrease (except F0)

Figure 1

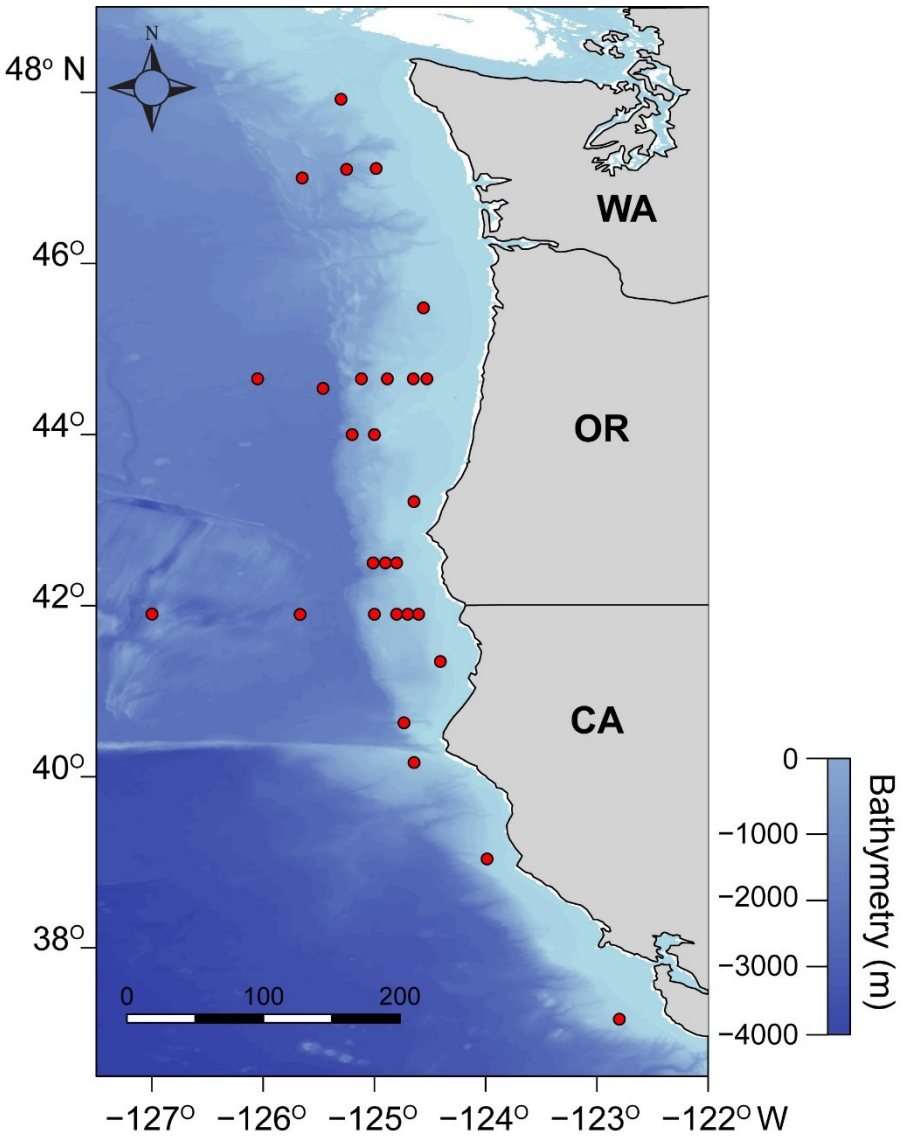
N
48° N
46°
44°
42°
40°
38°
WA
OR
CA
0
100
200
0
−1000
−2000
−3000
−4000
Bathymetry (m)
−127°
−126°
−125°
−124°
−123°
−122° W

Figure 2

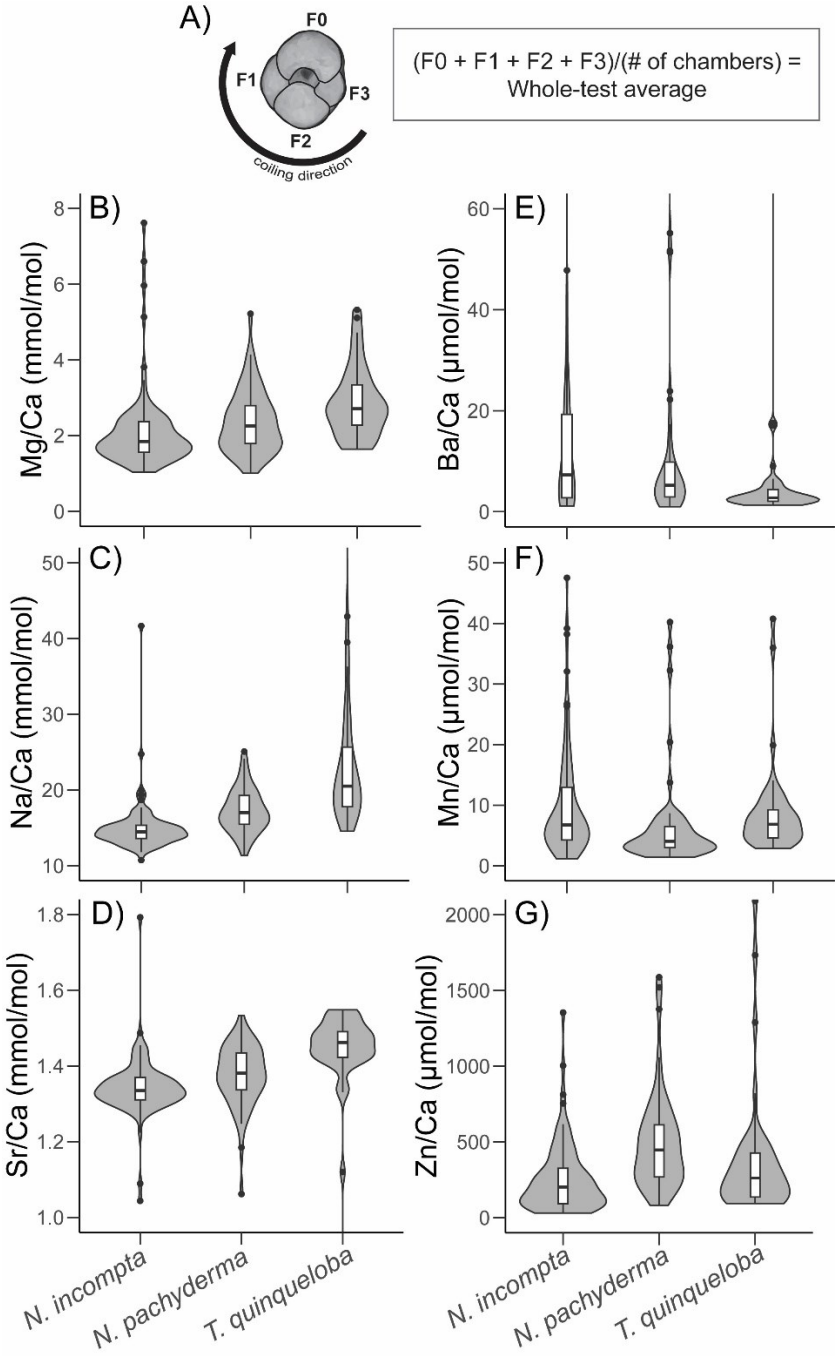
A)
F0
F1
F3
F2
coiling direction
(F0 + F1 + F2 + F3)/(# of chambers) = Whole-test average
B)
Mg/Ca (mmol/mol)
C)
Na/Ca (mmol/mol)
D)
Sr/Ca (mmol/mol)
E)
Ba/Ca (µmol/mol)
F)
Mn/Ca (µmol/mol)
G)
Zn/Ca (µmol/mol)
N. incompta
N. pachyderma
T. quinqueloba

Figure 3.

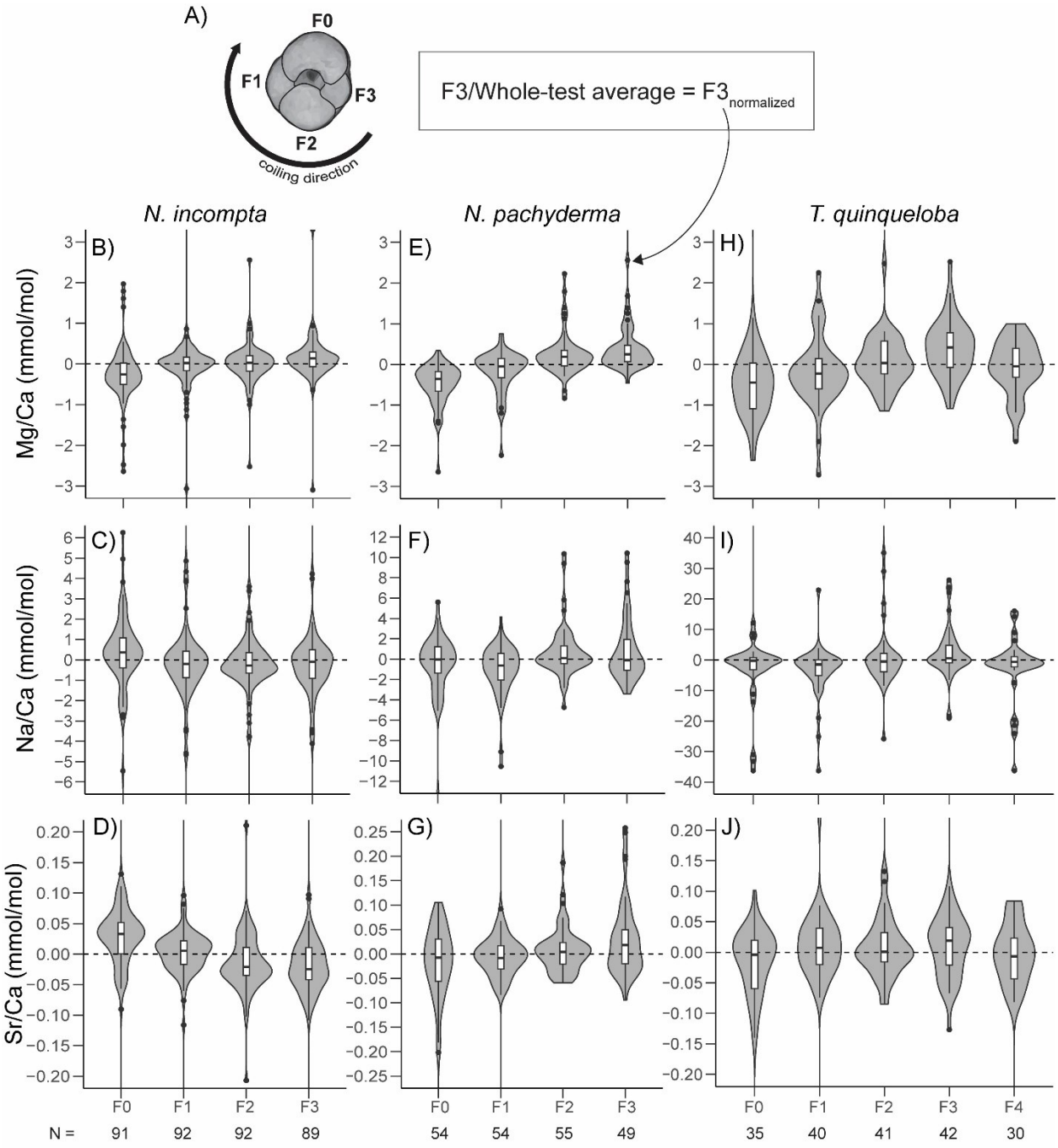
A)
F0
F1
F3
F2
coiling direction
F3/Whole-test average = F3 normalized
N. incompta
N. pachyderma
T. quinqueloba
B)
E)
H)
C)
F)
I)
D)
G)
J)
Mg/Ca (mmol/mol)
Na/Ca (mmol/mol)
Sr/Ca (mmol/mol)
F0 F1 F2 F3
N = 91 92 92 89
F0 F1 F2 F3
54 54 55 49
F0 F1 F2 F3 F4
35 40 41 42 30

Figure 4.

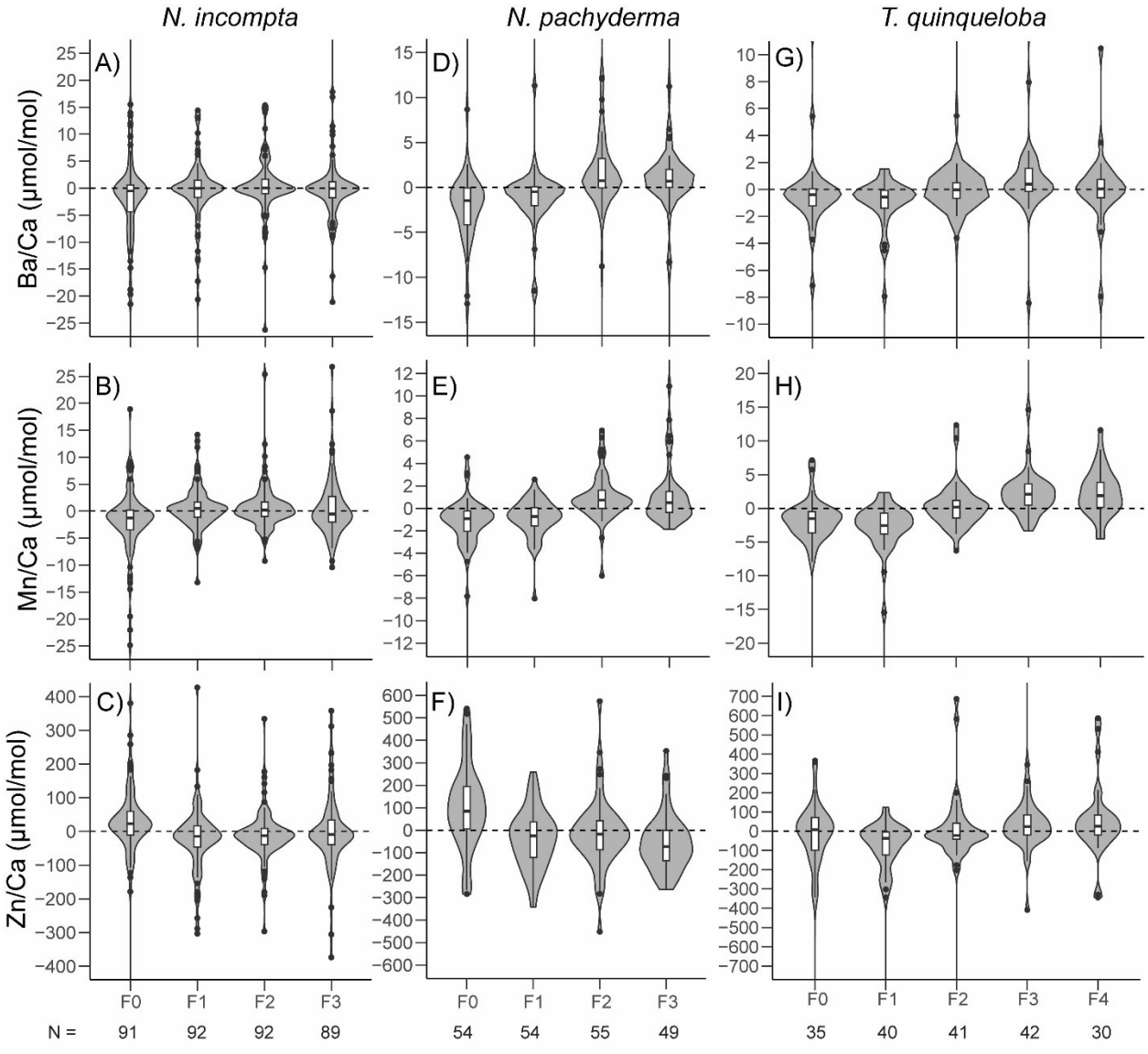
N. incompta
N. pachyderma
T. quinqueloba
A)
B)
C)
D)
E)
F)
G)
H)
I)
Ba/Ca (µmol/mol)
Mn/Ca (µmol/mol)
Zn/Ca (µmol/mol)
F0
F1
F2
F3
F4
N =
91
92
92
89
54
54
55
49
35
40
41
42
30

Figure 5.

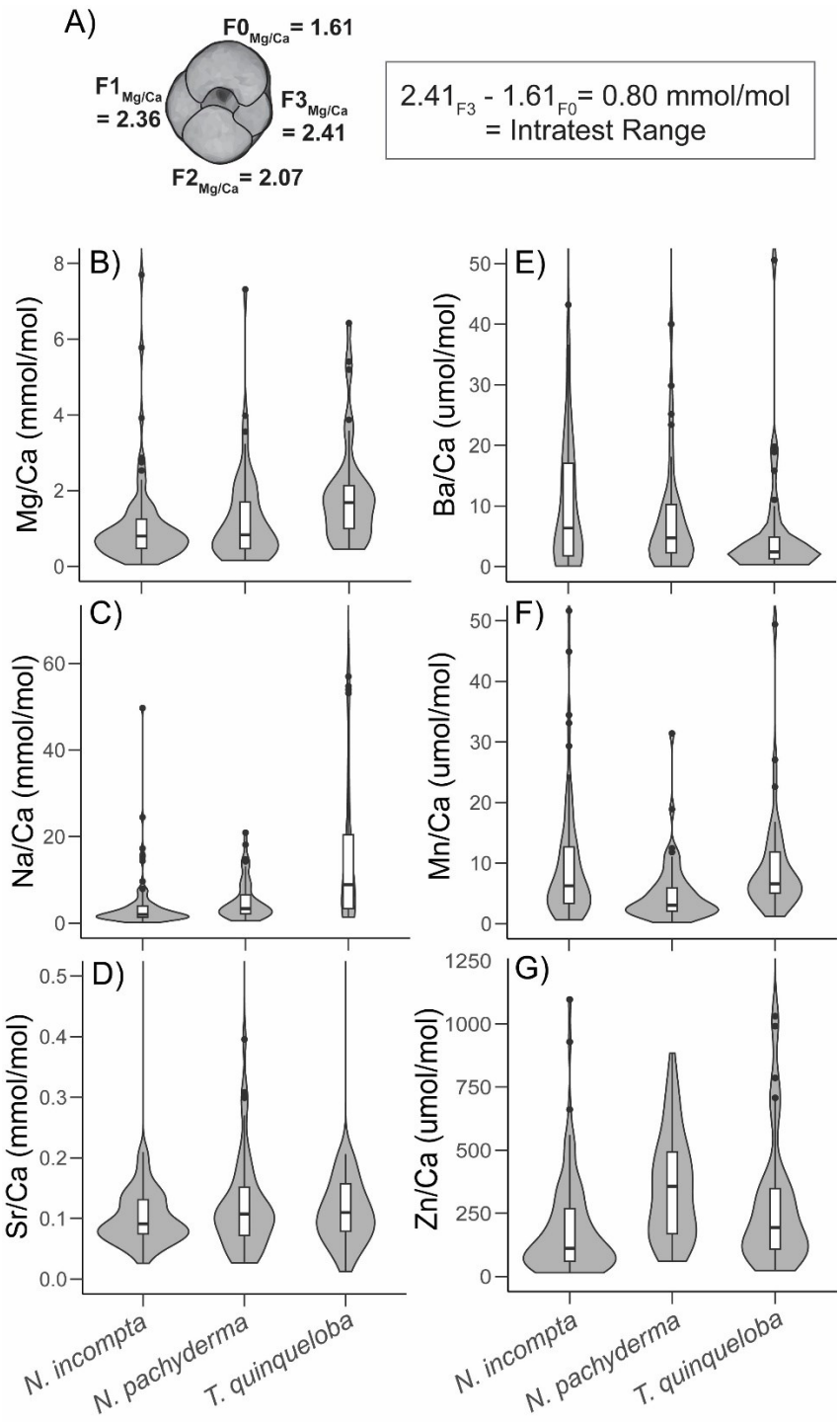
A)
F0Mg/Ca = 1.61
F1Mg/Ca = 2.36
F3Mg/Ca = 2.41
F2Mg/Ca = 2.07
2.41F3 - 1.61F0 = 0.80 mmol/mol
= Intratest Range
B)
Mg/Ca (mmol/mol)
C)
Na/Ca (mmol/mol)
D)
Sr/Ca (mmol/mol)
E)
Ba/Ca (umol/mol)
F)
Mn/Ca (umol/mol)
G)
Zn/Ca (umol/mol)
N. incompta
N. pachyderma
T. quinqueloba

Figure 6.

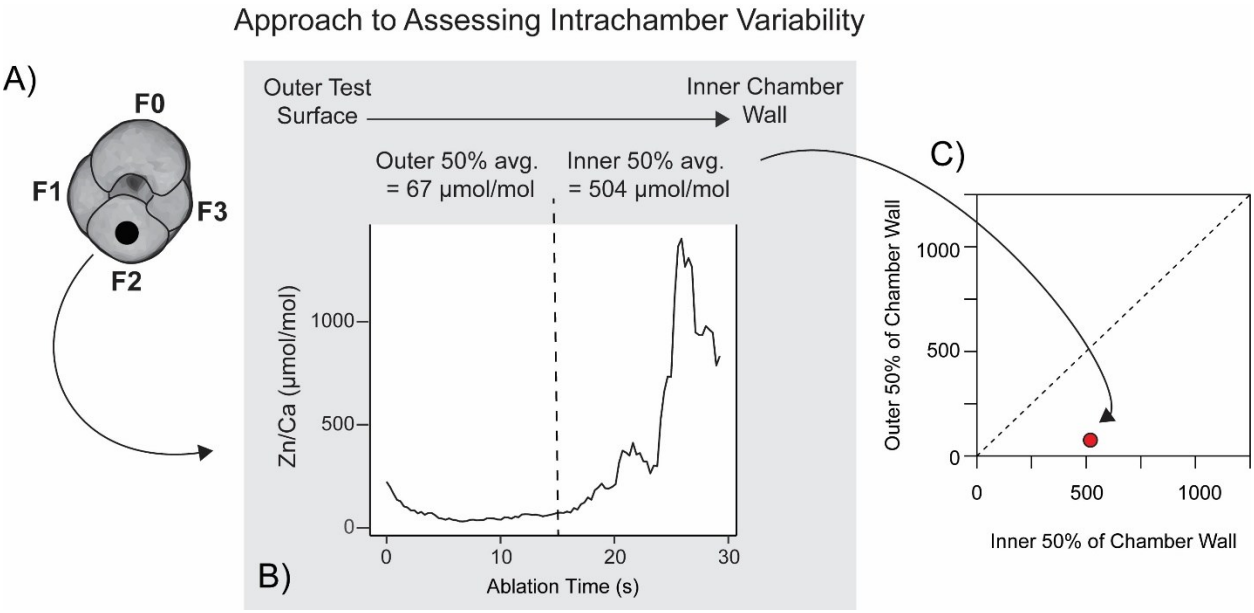
Approach to Assessing Intrachamber Variability
A)
F0
F1
F3
F2
Outer Test Surface
Inner Chamber Wall
Outer 50% avg. = 67 µmol/mol
Inner 50% avg. = 504 µmol/mol
Zn/Ca (µmol/mol)
1000
500
0
0
10
20
30
Ablation Time (s)
B)
C)
Outer 50% of Chamber Wall
1000
500
0
0
500
1000
Inner 50% of Chamber Wall

1319 **Figure 7**

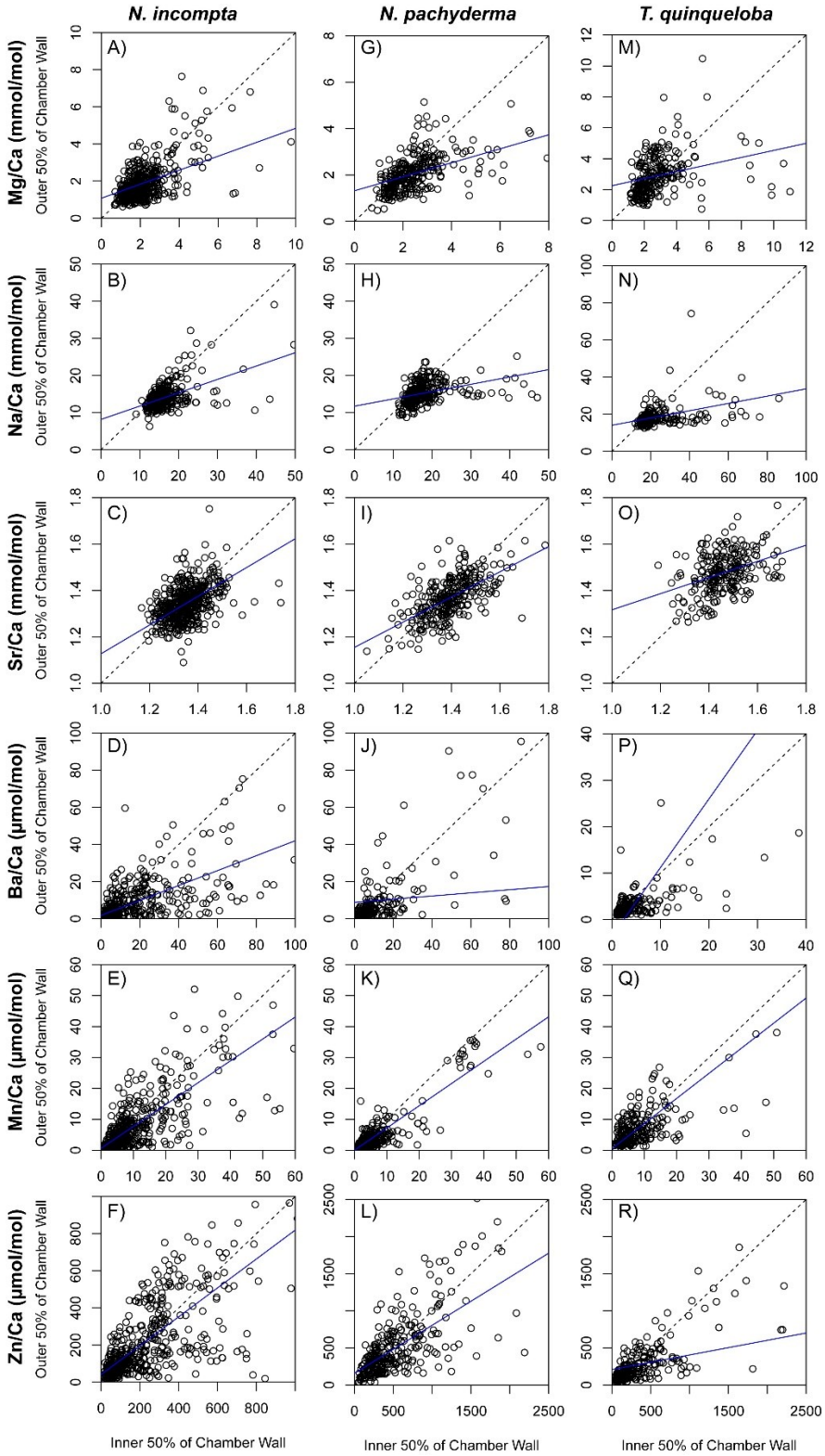

1320 .

1321

1322 **Figure 8.**

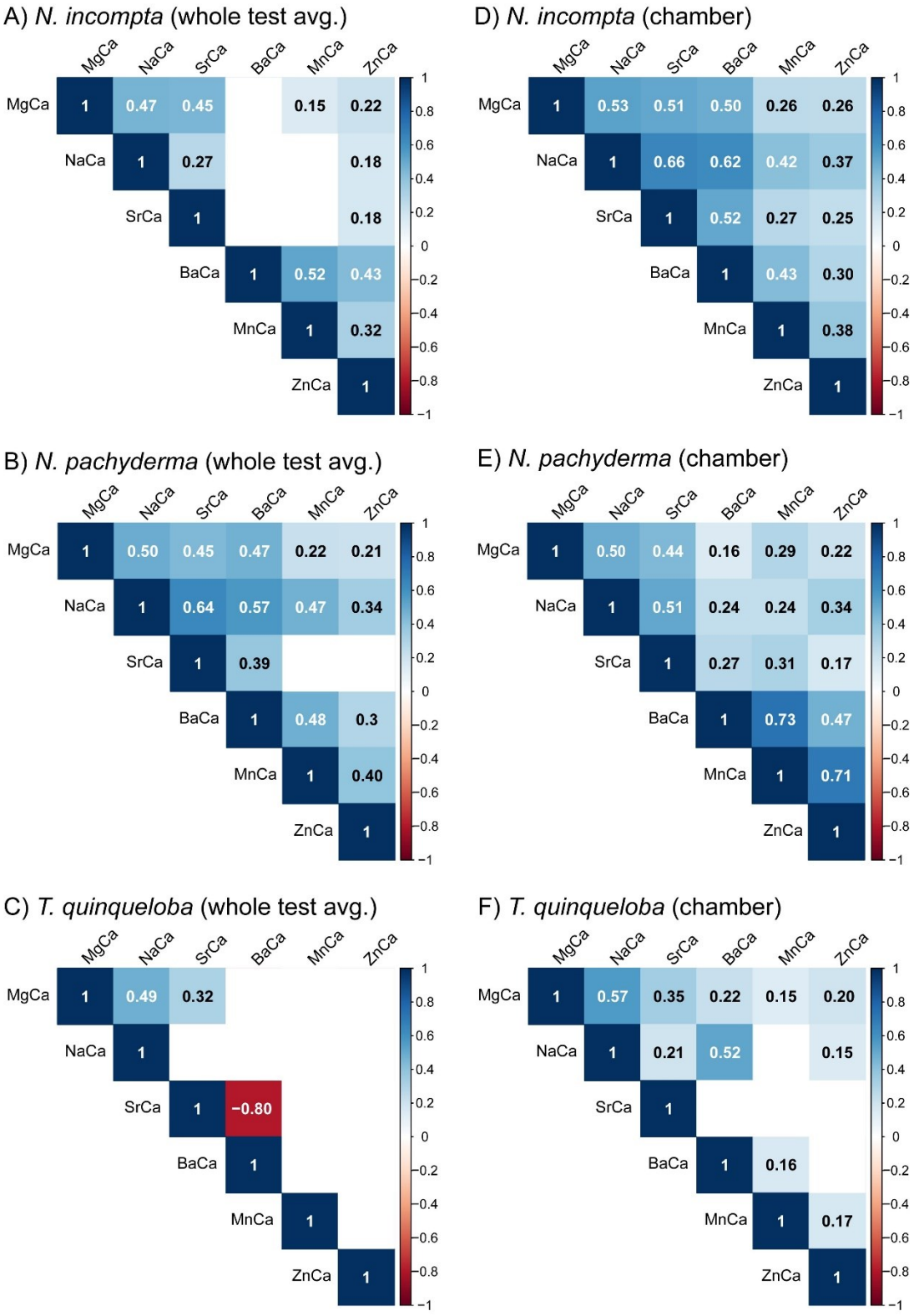

1323

1324